Contract No. FO4703-91-C-0112
RTI Report No. RTI/5180/60-31F
April 13, 1995

Casualty Areas from Impacting Inert Debris for People in the Open

Final Report

Prepared for

Department of the Air Force
45th Space Wing (AFSPC)
Directorate of Safety - 45 SW/SE
Patrick AFB, FL 32925

and

Department of the Air Force
30th Space Wing (AFSPC)
Directorate of Safety - 30 SW/SE
Vandenberg AFB, CA 93437

Contract No. FO4703-91-C-0112
Task No. 10/94-60

RTI Report No. RTI/5180/60-31F
April 13, 1995

Casualty Areas from Impacting Inert Debris for People in the Open

Final Report

Prepared by

Robert M. Montgomery
James A. Ward, Jr.

of

Research Triangle Institute
Center For Aerospace Technology
Launch Systems Safety Department

Prepared for

Department of the Air Force
45th Space Wing (AFSPC)
Directorate of Safety - 45 SW/SE
Patrick AFB, FL 32925

and

Department of the Air Force
30th Space Wing (AFSPC)
Directorate of Safety - 30 SW/SE
Vandenberg AFB, CA 93437

REPORT DOCUMENTATION PAGE

Form Approved
OMB No. 0704-0188

1. AGENCY USE ONLY (Leave blank)	2. REPORT DATE	3. REPORT TYPE AND DATES COVERED
	April 13, 1995	Final

4. TITLE AND SUBTITLE
Casualty Areas from Impacting Inert Debris for People in the Open

5. FUNDING NUMBERS
C: FO4703-91-C-0112
TA: 10/94-60

6. AUTHOR(S)
Robert M. Montgomery
James A. Ward, Jr.

7. PERFORMING ORGANIZATION NAME(S) AND ADDRESS(ES)
Research Triangle Institute*
3000 N. Atlantic Avenue
Cocoa Beach, FL 32931

ACTA, Inc.**
Skypark 3
23430 Hawthorne Blvd., Suite 300
Torrance, CA 90505

8. PERFORMING ORGANIZATION REPORT NUMBER
RTI/5180/60-31F

9. SPONSORING / MONITORING AGENCY NAME(S) AND ADDRESS(ES)
Department of the Air Force (AFSPC)
30th Space Wing
Vandenberg AFB, CA 93437
Mr. Martin Kinna (30 SW/SEY)

45th Space Wing
Patrick AFB, FL 32925
Louis J. Ullian, Jr. (45 SW/SED)

10. SPONSORING / MONITORING AGENCY REPORT NUMBER

11. SUPPLEMENTARY NOTES
* Subcontractor
**Prime Contractor

12a. DISTRIBUTION / AVAILABILITY STATEMENT
Distribution authorized to US Government agencies and their contractors to protect administrative/operational use data, 13 April 95. Other requests for this document shall be referred to the 30th Space Wing (AFSPC) Directorate of Safety (30 SW/SE), Vandenberg AFB, CA 93437, or 45th Space Wing (AFSPC), Directorate of Safety (45 SW/SE), Patrick AFB, FL 32925.

12b. DISTRIBUTION CODE

13. ABSTRACT *(Maximum 200 words)*

In a typical missile or space-vehicle risk study, a significant portion of the risk is due to falling inert debris. The report presents methods and procedures for estimating the casualty areas for such debris for people in the open, but not for people in houses, office buildings, or other structures.

After discussing what constitutes a hazardous piece and presenting the equation for computing casualty expectancy, detailed methods are provided for evaluating the basic casualty area for an impacting piece. This area depends on the cross-sectional area of the piece, the assumed dimensions of a person in the open, and the path angle of the velocity vector at impact. Other augmenting effects that can cause the casualty area of an impacting piece to be considerably larger than the basic casualty area of the piece itself are also discussed. These are: slide or skid, bounce or ricochet, splattering and cratering. A procedure for arriving at a composite casualty area to substitute in the casualty-expectancy equation is provided. Casualty areas for inert debris produced by breakup of the Atlas IIAS and Delta-GEM vehicles are given in appendices.

14. SUBJECT TERMS	15. NUMBER OF PAGES
inert launch-vehicle debris, casualty area	71
	16. PRICE CODE

17. SECURITY CLASSIFICATION OF REPORT	18. SECURITY CLASSIFICATION OF THIS PAGE	19. SECURITY CLASSIFICATION OF ABSTRACT	20. LIMITATION OF ABSTRACT
Unclassified	Unclassified	Unclassified	SAR

Abstract

In a typical missile or space-vehicle risk study, a significant portion of the risk is due to falling inert debris. The report presents methods and procedures for estimating the casualty areas for such debris for people in the open, but not for people in houses, office buildings, or other structures.

After discussing what constitutes a hazardous piece and presenting the equation for computing casualty expectancy, detailed methods are provided for evaluating the basic casualty area for an impacting piece. This area depends on the cross-sectional area of the piece, the assumed dimensions of a person in the open, and the path angle of the velocity vector at impact. Other augmenting effects that can cause the casualty area of an impacting piece to be considerably larger than the basic casualty area of the piece itself are also discussed. These are:

a. slide or skid
b. bounce or ricochet
c. splattering and cratering

A procedure for arriving at a composite casualty area to substitute in the casualty-expectancy equation is provided.

Casualty areas for inert debris produced by breakup of the Atlas IIAS and Delta-GEM vehicles are given in appendices.

Table of Contents

Table of Figures

Table of Tables

Casualty Areas from Impacting Inert Debris for People in the Open

1. Introduction

When a missile or space vehicle malfunctions, people and facilities may be subjected to significant risks from falling inert debris, or from overpressures and secondary debris produced by a stage, component, or large propellant chunk that explodes on impact. Although risks are greatest in the launch area and along the intended flight line, lesser risks exist throughout the area inside the impact limit lines, and even outside if the flight termination system should fail or other unlikely events occur. In accordance with contractual tasking, the purpose of this study is to develop analytic models for estimating casualty expectancy from primary (impacting) and secondary (projected) inert debris for people in the open. As used here, primary debris consists of non-explosive vehicle components and pieces that fall to earth following a vehicle malfunction. Secondary debris consists of inert vehicle fragments and crater materials projected outward from impacting components. Damage to facilities and injuries to people from explosive overpressures have been treated in a companion document[1], "Facility Damage and Personnel Injury From Explosive Blast". Although fire, toxic materials, and radiation may also subject personnel to significant danger, these hazards are not addressed in Ref. [1] or in this study.

2. Casualty Expectancy

2.1 The Casualty Expectancy Concept

If inert vehicle pieces impact in an area or region of constant population density, the expected or average number of casualties can be calculated from the so-called casualty-expectancy equation,

$$E_c = P_I \times N \times \frac{A_c}{A} \tag{1}$$

where E_c is the expected number of casualties, P_I is the probability of impact in the region, N is the number of people in the region, A_c is the total effective casualty area for the impacting pieces, and A is the area of the region. This equation, which is also applied when the population density is unknown or random, is used to calculate the expected number of casualties to people in the open from impacting inert debris. The actual calculation of casualty expectancy is considerably more involved than might be inferred from Eq. (1), since calculations must be summed statistically over all failure modes and time intervals for all pieces in each debris class and for all classes of debris.

It should be noted that E_c is not the probability of a casualty. The distinction between casualty expectancy and probability of casualty can be clarified by a simple numerical example: Assume for some vehicle system that one test in 1000 is expected to result in

injury to people and that, on the average, five people are injured in each accident. Then, the probability of casualty is 1/1000, whereas the casualty expectancy is 5/1000 or 1/200. In unusual situations, casualty expectancy may be greater than one, while the probability of casualty can never be.

2.2 Identification of Hazardous Pieces

An individual is considered a casualty if he is directly hit by a primary falling piece, or by a sufficiently energetic bouncing, ricocheting, or skidding piece, or by secondary crater ejecta or piece fragments projected outward from an impacting piece at velocities above some threshold value. In other words, if a person is physically occupying space which a moving fragment would otherwise pass through or impact upon, he or she is a casualty by this definition. This definition is not consistent with the one that has appeared in Air Force explosive safety standards[2], where a hazardous piece has been defined as one possessing 58 ft-lb of kinetic energy at impact. Presumably, this is the threshold for serious rather than minor injury, since a one-pound piece must fall at least 58 feet, or a 58-pound piece one foot, to acquire this kinetic energy. To put it another way, a one-pound piece must attain a speed of 61 ft/sec, a two-pound piece 43 ft/sec, and a 58-pound piece 8 ft/sec to have kinetic energies of 58 ft-lb. Such energetic pieces might well be permanently disabling or lethal.

If any person who is hit is regarded as a casualty, the seeming effect is to consider all falling pieces as hazardous, i.e., to set the kinetic-energy threshold at zero foot-pounds. In application, this is not generally done, since light pieces with small ballistic coefficients may not be included in the vehicle breakup data, or they may be eliminated from the risk calculations by the safety analyst. The difficulty in establishing a suitable threshold is pointed out on page 1-10 of an ACTA report[3], where a tackled football player who experiences an energetic impact of 400-500 foot-pounds is typically uninjured, while an individual stopping a 38-caliber bullet having a kinetic energy of only 120 foot-pounds may well be killed. As another example of why kinetic energy alone is not a good indicator of hazard, a vehicle skin piece having an area of one square foot and a tumbling ballistic coefficient of two has a vertical velocity component at impact of about 21 ft/sec and a kinetic energy of about 8 ft-lbs. A broad-side impact from such a piece may leave a person unscathed, while a slashing end-on impact may result in a serious wound.

In view of the foregoing difficulties in establishing suitable kinetic-energy thresholds, RTI regards all pieces included in the hit-probability and casualty-expectancy calculations as hazardous to people in the open. It is left to the analyst to avoid ultra conservatism by eliminating from the calculations any pieces that present negligible risks.

3. Casualty-Area Computations

The casualty area associated with an impacting piece or component is a theoretical region on the ground within which 100 percent casualties occur and outside of which no one is injured. In reality, no such physical area exists. Rather the effective casualty area, as developed in this study, is a numerical quantity which, on the average, gives the proper answer in the casualty-expectancy equation. (The terms 'effective casualty area' and 'casualty area' will be used interchangeably.)

For people in the open, the effective casualty area for an impacting inert piece may be considerably larger than the maximum cross-sectional area of the piece itself to account for the following:

a. dimensions of a person,
b. wind and trajectory path angle,
c. slide or skid,
d. bounce or ricochet,
e. splattering and cratering.

For every falling piece, the dimensions of a person (item a) and the effect of trajectory path angle at impact (item b) must be included in the casualty-area evaluation. As shown later, both items are accounted for in a single equation to produce a **basic casualty area** for the piece. The three supplemental effects of slide, bounce, and splatter are considered to be mutually exclusive. One of the three is assumed to occur even though in unusual cases an impacting piece may bury itself without ejecting debris beyond the rim of the impact area. The casualty areas associated with all three supplemental effects are evaluated, and a **composite casualty area** obtained by adding the largest of the three to the basic casualty area. For application in RTI's risk computation program, facility **DAM**age and **P**ersonnel injury (DAMP), the composite casualty areas for inert debris for people in the open are computed off-line for each class of debris. The areas are input to DAMP as a function of time from launch.

The five effects (a through e above) that must be accounted for in evaluating the effective casualty area for an inert piece for a person in the open are discussed individually in the sections that follow.

For people in buildings or shelters, the casualty area of a piece may be larger or smaller than its maximum cross-sectional area, depending on the capability of the piece to penetrate or perforate the structure. If the piece is incapable of penetrating or causing internal structural damage, the effective casualty area for the piece is zero for that structure. Thus for a sheltered person, the effective casualty area associated with a falling inert piece must account for:

a. capability of piece to penetrate or perforate the structure,

b. effects of excess kinetic energy retained by the primary inert piece if perforation occurs,
c. falling structural debris produced when the inert piece impacts on the structure.

The casualty-area modeling in subsequent sections of this report does not address these items. Procedures for estimating inert-debris casualty areas for people in structures are being developed in a separate study by ACTA, Inc.

4. Dimensions of a Person

In calculating casualty area, each person is assumed to be a vertically-oriented, right circular cylinder h_p feet high with a radius of r_p. Values of h_p and r_p are typically set to six feet and one foot, respectively. This is obviously a compromise, since some people are shorter and some taller than six feet, and since a person standing erect has a cross-sectional area somewhat less than π square feet, while a person sitting or prone occupies a greater area. Within reasonable limits, the configuration assumed for a person is not significant, since the effects of minor variations in size or shape are overwhelmed by the uncertainties in the overall process (e.g., the actual number of falling pieces). All vehicle pieces are assumed to be circular with the area of each piece equal to the pieces's largest cross-sectional area.

With the forgoing assumptions – and no other considerations for the present – the casualty area for a vertically falling fragment must be made larger than its cross-sectional area to account for the dimensions of a person. The concept is illustrated in Fig. 1 where r_f is the radius of a circularized impacting fragment and r_p is the radius of a person. If the center of the fragment falls within the circle of radius $(r_p + r_f)$ centered at A, the person will be hit. To put it another way, any person whose geometric center lies within a circle of radius $(r_p + r_f)$ centered at B will be hit.

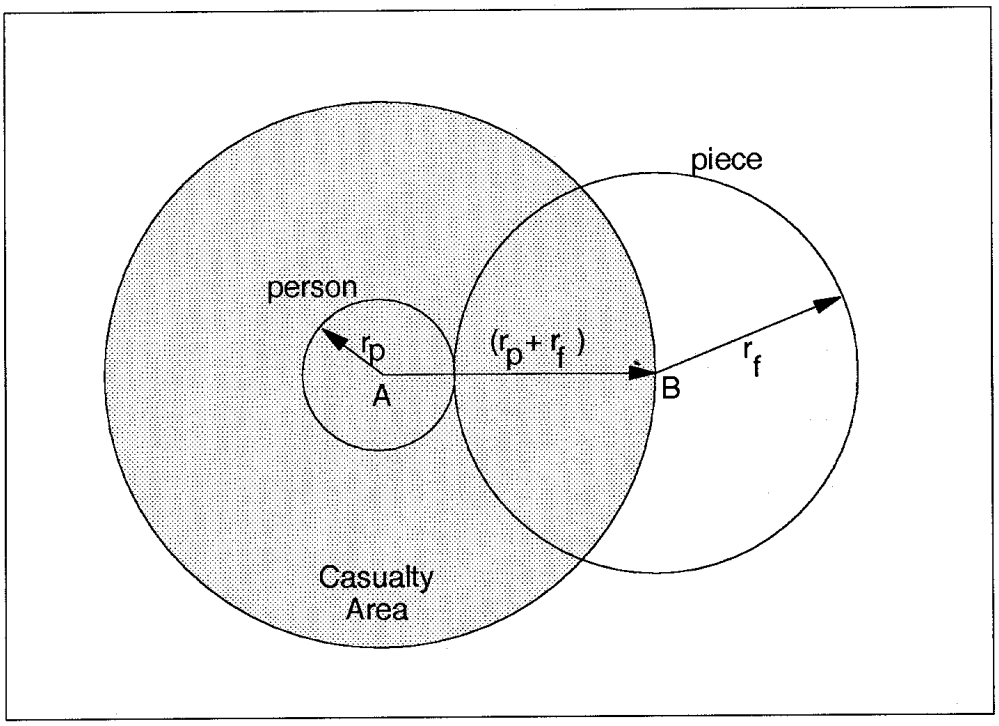

Figure 1. Casualty Area for Piece Falling Vertically

In either case, the casualty area for the piece due solely to the dimensional effects of a person and the cross-sectional area of the piece becomes

$$A_c(\text{vertical}) = \pi\left(r_p + r_f\right)^2 \tag{2}$$

where r_f is the circularized radius of the piece and r_p is the radius of a person.

5. Wind and Path Angle Effects

In general, vehicle pieces do not fall vertically as postulated in Section 4. Rather, the velocity vector v at impact makes some angle γ with respect to the horizontal, since (1) not even the no-wind trajectory is vertical at impact although it may be nearly so for pieces with low ballistic coefficients, and (2) existing or assumed winds produce an additional horizontal velocity component during descent. As a result of the horizontal component of velocity, the area swept out during the last h_p feet of fall can cause the casualty area for any piece to be considerably larger than the casualty area obtained for a purely vertical fall.

Figure 2 depicts two positions of a circularized flat piece, one when it is h_p feet above ground and the other at impact. A plan view is shown at the bottom of the figure, with a side view above it.

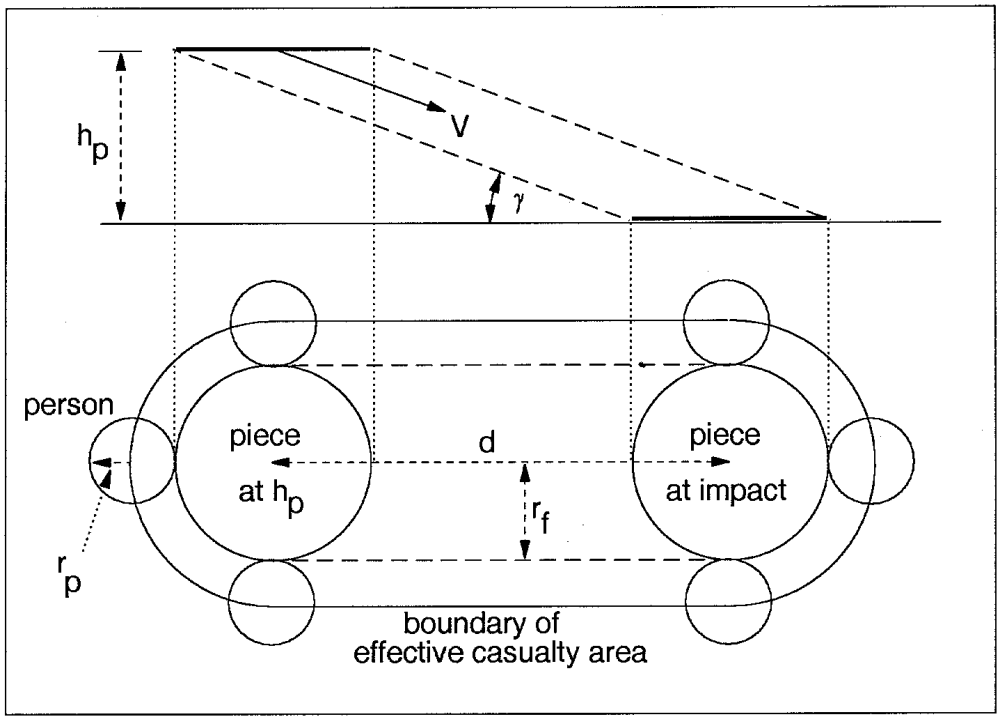

Figure 2. Casualty Area for Piece Falling Diagonally

Throughout the last h_p feet of fall, the motion is assumed to be translational with the piece oriented so that its largest cross-section is parallel to the ground. The horizontal distance between centers of the two positions is seen to be

$$d = \frac{h_p}{\tan\gamma} \tag{3}$$

where d is the horizontal distance traveled by the piece in falling from height h_p, and γ is the average path angle of the velocity vector relative to the horizontal during the fall.

Circles of radius r_p representing a person have been circumscribed about the outer boundary swept out by the falling piece. Assuming no perturbations upon impact, the area inside the curve drawn through the centers of the bounding circles represents the effective casualty area, since any person whose geometric center lies inside this area is hit, and any person whose center is outside is not.

The effective casualty area due to wind and path angle effects is seen to be

$$A_c \text{ (impact angle)} = 2(r_p + r_f)d + \pi(r_p + r_f)^2 \tag{4}$$

where r_p is the radius of a person, r_f is the piece radius, and d is given by Eq. (3). Previously, the area given by Eq. (4) was called the **basic casualty area** for the piece.

The effects that impact path angle and fragment size have on casualty area are shown in Table 1. For these computations r_p is 1.0 foot and h_p is 6.0 feet. The table entries show the ratios of the casualty areas computed from Eq. (4) (shown in Fig. 2) to those from Eq. (2) (shown in Fig. 1) for various path angles.

Table 1. Effect of Impact Path Angle on Casualty Area

Fragment Radius (ft)	Ratio of Areas					
	$\gamma = 90°$	$\gamma = 88°$	$\gamma = 85°$	$\gamma = 80°$	$\gamma = 70°$	$\gamma = 50°$
0.5	1.00	1.09	1.22	1.45	1.93	3.14
1.0	1.00	1.07	1.17	1.34	1.70	2.60
2.0	1.00	1.04	1.11	1.22	1.46	2.07
3.0	1.00	1.03	1.08	1.17	1.35	1.80
4.0	1.00	1.03	1.07	1.13	1.28	1.64
5.0	1.00	1.02	1.06	1.11	1.23	1.53
6.0	1.00	1.02	1.05	1.10	1.20	1.46
8.0	1.00	1.01	1.04	1.07	1.15	1.36
10.0	1.00	1.01	1.03	1.06	1.13	1.29

6. Slide or Skid

After impact, a body that slides or skids along the surface in coming to rest is unlikely to do so smoothly. More likely, its motion will be some complicated combination of slide, skid, tumble, roll, and bounce that defies accurate analysis. To estimate the additional casualty area that such motion produces, the travel distance is calculated as though the body were in pure slide, thus resulting in constant deceleration. To avoid underestimation of the distance, conservative slide coefficients must be chosen.

In estimating slide distances, two types of surfaces are considered, namely, a hard (presumably regular) surface and a soft (perhaps irregular) surface. Except for the assigned coefficients of friction, the slide calculations are the same for both surfaces. In estimating the casualty area due to slide for people in the open, the type of surface for each group of people must be specified. If the type is unknown or not indicated, the assumption is made that the surface is hard.

6.1 Slide Equations

Given the initial horizontal component of velocity at impact and the coefficient of sliding friction between a moving and a stationary body in constant contact, the distance the

moving body travels before coming to rest can be computed from the following equations found in elementary physics books:

$$
\begin{aligned}
F &= -f\,w \\
a &= \left(\frac{g}{w}\right)F = -f\,g \\
t &= \frac{0 - v_h}{a} = \frac{v_h}{f\,g} \\
d_s &= \frac{1}{2}a\,t^2 + v_h\,t = \frac{1}{2}\left(\frac{v_h^2}{f\,g}\right)
\end{aligned}
\qquad (5)
$$

where F is the frictional force, f is the coefficient of friction, w is the body weight, a is the horizontal acceleration, g is the acceleration due to gravity, t is the time required to bring the sliding body to rest, v_h is the initial horizontal velocity, and d_s is the slide distance.

6.2 Slide Coefficients and Distances

Typical values for the coefficient of sliding friction between various pairs of materials are shown in Table 2[4]. Coefficients could not be found for metals on sand, shell, concrete, blacktop, or gravel.

Table 2. Coefficients of Sliding Friction

Materials	Coefficient of Friction, f
masonry on brickwork	0.60 to 0.70
wood on wood	0.25 to 0.50
iron on stone	0.30 to 0.70
wood on stone	0.40
metals on oak	0.50 to 0.60
metals on metals	0.15 to 0.30
masonry on clay	0.33 to 0.51
earth on earth, gravel	0.81 to 1.11

Table 3 shows slide distances for six values of f for initial horizontal velocities up to 25 ft/sec. It is apparent that the casualty area due to slide depends on the horizontal velocity component at impact.

Table 3. Horizontal Slide Distance

Initial Horizontal Speed (ft/sec)	Horizontal Slide Distance (ft)					
	f = 0.3	f = 0.4	f = 0.5	f = 0.6	f = 0.7	f = 0.8
5	1.3	1.0	0.8	0.6	0.6	0.5
10	5.2	3.9	3.1	2.6	2.2	1.9
15	11.7	8.7	7.0	5.8	5.0	4.4
20	20.7	15.5	12.4	10.4	8.9	7.8
25	32.4	24.3	19.4	16.2	13.9	12.1

Although in theory the computation of slide distance is straightforward, major uncertainties arise in applying the procedures to impacting vehicle fragments or components:

(a) Immediately after impact, there is no suitable way to estimate the residual horizontal velocity of a sliding fragment;

(b) The impacted surface may be irregular and non-homogeneous, so the deceleration during the stopping period may vary considerably;

(c) The coefficient of friction between a deformed body and an unknown surface cannot be accurately estimated, and surely is not constant;

(d) While coming to rest, a body that is primarily sliding may also roll, bounce, tumble, or dig into the surface.

Since a soft surface is more likely to be irregular than a hard surface, and since an impacting body is more likely to dig into a soft surface as it slides or tumbles along, it seems reasonable to assume that the coefficient of friction, on average, is higher for soft surfaces. At some impact velocity, slide is unlikely to occur either because the impacting body digs into a soft surface, or bounces or shatters following a hard-surface impact. The no-slide velocity varies widely depending primarily on the composition of the impacting body and its attitude at impact. Although no real justification exists, a constant no-slide threshold for the vertical velocity component has been chosen, since there seems to be little point in postulating some artificial density function for the threshold.

6.3 Assumptions

Although all of the above factors contribute to the uncertainty of the result, quasi slide cannot be discarded as an impossibility, particularly early in flight or for low-velocity fragments that impact at any time on hard surfaces such as concrete, blacktop, packed

shell, or rock. So that the casualty areas due to slide will not be underestimated, the following assumptions have been made:

(1) The vertical component of velocity after impact is zero.

(2) The horizontal component of velocity is unchanged by impact.

(3) For all fragments, the average coefficient of friction f is 0.5 for slides on hard surfaces, corresponding to the mid-range value shown in Table 3 for iron on stone. For slides on soft surfaces f is 0.7, a value at the lower end of the range for earth on earth or gravel.

(4) If the vertical component of impact velocity exceeds 100* feet per second, the impacting body will not slide, and the casualty area due to slide is zero.

(5) The slide distance can be evaluated using Eqs. (5) when the vertical component of impact velocity is less than 100 feet per second. The computed sliding distance is interpreted to mean the maximum hazardous distance rather than the maximum possible distance.

---

* At vertical velocities exceeding 100 feet per second, an impacting body is expected to break up, bounce, or dig into the surface rather than slide. As defined in this report, these events are mutually exclusive.

6.4 Casualty Area for Slide or Skid

The computation of casualty area due to slide is illustrated in Fig. 3, where the sliding fragment of radius r_f has been augmented by the radius of a person r_p, and d_s is the slide distance computed from Eqs. (5).

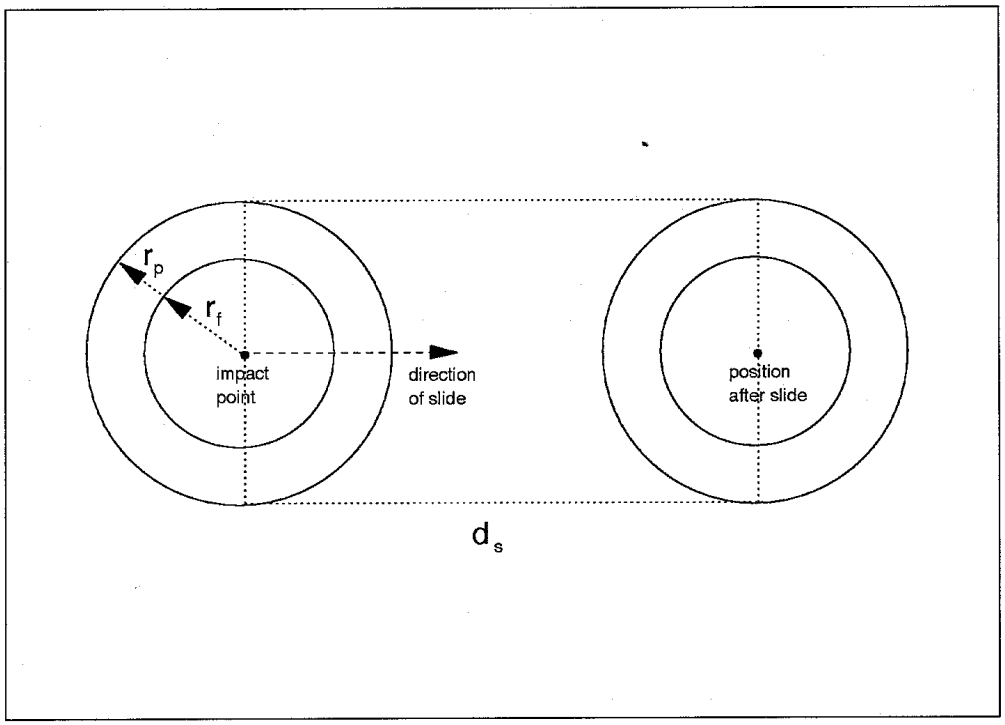

Figure 3. Casualty Area Due to Slide

The additional casualty area due to slide is

$$A_c(\text{slide}) = 2(r_f + r_p)d_s \tag{6}$$

In evaluating A_c(slide), the area $(\pi/2)(r_f + r_p)^2$ is both added and subtracted from the right-hand member of Eq. (6). It is added to account for the semi-circular area occupied by the leading half of the augmented fragment at its position after slide; the same area must also be subtracted to avoid counting it twice, since the area occupied by the leading half of the augmented fragment at impact has already been accounted for in the basic casualty area given by Eq. (4).

Although Fig. 3 depicts the case where $d_s > r_f + r_p$, exactly the same result is obtained if $d_s \leq r_f + r_p$.

7. Bounce or Ricochet

Since falling pieces have both vertical and horizontal components of velocity, bodies that remain essentially intact after impact may bounce or ricochet along the impacted surface, thereby increasing their effective casualty areas. If a body breaks up and disperses upon impact, it is not considered as a bouncing body even though some dispersing fragments do in fact bounce. Instead, the dispersing or bouncing fragments are treated as splatter fragments, and the additional casualty area due to splattering is calculated as discussed in a later section (Section 8) of this report. For pieces with small ballistic coefficients and thus low impact velocities, bounce and slide are probably indistinguishable from ricochet. Except for the effects of wind, such pieces would impact nearly vertically. Even pieces with large ballistic coefficients are likely to impact at high path angles with respect to the horizontal, except possibly early in flight when vehicle breakup may result in relatively high horizontal velocities at impact. For steep path angles, ricochet is unlikely to occur but, if it should, would appear as an integral part of splattering, bounce, or slide. For these reasons, the casualty area due to possible ricochet was assumed to be a part of one of these effects.

It is certainly possible for an impacting piece to bounce more than once. Because of the uncertainty in the overall process, bouncing pieces are considered to be hazardous during the first bounce only.

In estimating casualty area due to bounce, both hard and soft surfaces are considered. Except for the functions used to define the coefficients of restitution, the procedures and equations for the two surfaces are identical. In making risk calculations for people in the open, the type of surface on which each person or group of people is located must be specified. If the type is unknown or not indicated, the assumption is made that the surface is hard.

7.1 Bounce Equations

A rough estimate of bounce distance can be made by estimating the rebound velocity after impact. In general, the rebound velocity for a body may be calculated as

$$v(\text{rebound}) = e\sqrt{v_v^2 + v_h^2} \tag{7}$$

where e is the coefficient of restitution, and v_v and v_h are the vertical and horizontal components of velocity at impact. If the angles of impact and rebound are equal, then

$$\phi(\text{rebound}) = \tan^{-1}\left(\frac{v_v}{v_h}\right) \tag{8}$$

where ϕ is measured relative to the horizontal. Since, for the present, the impact and rebound angles are assumed to be equal, the vertical and horizontal components of rebound velocity are

$$v_{vr} = e\, v_v$$
$$v_{hr} = e\, v_h \tag{9}$$

The vertical component of rebound velocity can be used to compute the time to second impact by

$$t = \frac{2\, v_{vr}}{g} \tag{10}$$

and the horizontal travel distance to second impact is given by

$$d_b = v_{hr}\, t = \frac{2\, e^2\, v_h\, v_v}{g} \tag{11}$$

where g is the acceleration due to gravity.

7.2 Horizontal Bounce Distance

At low impact velocities, the energy (and hence velocity) lost in deforming an impacting body and scarring the surface is relatively small, leading to a coefficient of restitution somewhat higher than that for high-velocity impacts. For iron on iron, lead on lead, and iron on lead, approximate values of e[5] within some unspecified (but surely low) velocity domain are 0.66, 0.20, and 0.14, respectively. During an inelastic impact where the impacted body is relatively large and at rest, the kinetic energy (KE) lost by the falling body can be obtained by multiplying the KE at impact by $(1 - e^2)$. If a value of 0.4 is used for e, 84% of the impact KE is lost and 16% remains to produce bounce. If e = 0.2, 4% of the energy produces bounce. As a numerical example, consider a 100-pound piece impacting with a vertical velocity component of 20.9 ft/sec, (W/C_DA = 0.5 lb/ft^2), and a horizontal (wind) velocity of 11.5 ft/sec. If e = 0.4, 16% of the impact KE produces a rebound velocity of 9.5 ft/sec. The rebound angle is 61.2°, and the impact range is 2.4 feet. Table 4 shows bounce distances for six values of e and nine ballistic coefficients, assuming a horizontal velocity component at impact of 11.5 ft/sec, and a vertical velocity component equal to terminal velocity computed as follows:

$$V_T(\text{ft/sec}) = \sqrt{\left(\frac{2}{\rho_o}\right)\left(\frac{w}{C_d A}\right)} \tag{12}$$

where ρ_o is the atmospheric density at sea level in slugs/ft^3 (22.85×10^{-4} for the US Standard Atmosphere 1962), and (w/C_dA) is the ballistic coefficient β in lbs/ft^2.

Table 4. Bounce Distances

		Horizontal Bounce Distance (ft)*					
β (lbs/ft^2)	V_T (ft/sec)	e = 0.05	e = 0.1	e = 0.2	e = 0.3	e = 0.4	e = 0.6
0.2	13.2	0.02	0.09	0.4	0.9	1.5	3.4
0.5	20.9	0.04	0.15	0.6	1.3	2.4	5.4
1.0	29.6	0.05	0.21	0.8	1.9	3.4	7.6
2.0	41.8	0.07	0.30	1.2	2.7	4.8	10.8
5.0	66.2	0.12	0.47	1.9	4.3	7.6	17.0
10.0	93.6	0.17	0.67	2.7	6.0	10.7	24.1
20	132.3	0.24	0.95	3.8	8.5	15.1	34.0
50	209.2	0.37	1.50	6.0	13.5	23.9	53.8
100	295.8	0.53	2.12	8.5	19.0	33.8	76.1

* Based on vertical terminal velocity and a horizontal velocity component of 11.5 ft/sec

7.3 Height of Bounce

Since no experimental or theoretical data could be found in establishing values for e, a selection based on engineering judgement and intuition was necessary. To provide further insight, height of bounce was calculated from the equation

$$h_b = \frac{v_{vr}^2}{2g} \tag{13}$$

using the same ballistic coefficients and terminal velocities given in Table 4. The results are shown in Table 5 for six constant values of e.

Table 5. Bounce Heights

		Height of Bounce (ft)					
β (lbs/ft^2)	V_T (ft/sec)	e = 0.05	e = 0.1	e = 0.2	e = 0.3	e = 0.4	e = 0.6
0.2	13.2	0.01	0.03	0.11	0.24	0.43	0.97
0.5	20.9	0.02	0.07	0.27	0.61	1.09	2.44
1.0	29.6	0.03	0.14	0.54	1.22	2.18	4.90
2.0	41.8	0.07	0.27	1.09	2.45	4.35	9.79
5.0	66.2	0.17	0.68	2.72	6.12	10.9	24.5
10.0	93.6	0.34	1.36	5.44	12.2	21.8	49.0
20	132.3	0.68	2.72	10.9	24.5	43.5	97.9
50	209.2	1.70	6.80	27.2	61.2	109.	245.
100	295.8	3.40	13.6	54.4	122.	218.	490.

From inspection of Table 5, a body with β = 1.0 and e = 0.3 that impacts at 29.6 ft/sec would bounce about 1.2 feet high. Since to acquire this velocity such a body must fall from a height of at least 14 feet, a 1.2-foot-high bounce does not seem unreasonable. At the other extreme, a body with β = 100 and e = 0.3 impacting at a terminal velocity of 295.8 ft/sec would, according to the bounce equations, rebound 122 feet. This bounce height seems unreasonable, since a vehicle component impacting at this speed would surely shatter while producing a crater, or bury itself into or under the surface, or be flattened almost beyond recognition. In fact, it does not seem credible that vehicle components impacting at speeds of several hundred feet per second will remain essentially intact, and thus produce bounce, as defined in this report. (The added casualty area produced by the splattering of pieces from high-speed impacts is discussed later in Section 8.)

7.4 Estimates of Low-Velocity Coefficients of Restitution

As a further crude guide in estimating low-velocity values of e, several objects were dropped from a balcony onto a concrete sidewalk and then onto a weedy dirt surface. Items dropped from a height of about 9 feet included a fully-inflated basketball, a standard softball, a tennis ball, a small wood block, a steel bolt with flange nut attached, and a thin steel cup-like object with a small hole in the bottom. For the three balls, height of bounce was measured (within an inch or so), and the coefficient of restitution calculated from the equation

$$e = \sqrt{\frac{h}{H}} \tag{14}$$

where h and H are the rebound and drop heights, respectively.

For other dropped objects, a different procedure was used to estimate e, since bounce height and rebound angle were critically dependent on impact attitude. For each of several drops, the height and distance of bounce were measured (within an inch or so), and the rebound velocity needed to produce a trajectory with this apogee and distance was calculated. The impact velocity for a 9-foot drop was then determined, and e calculated from the equation

$$e = \frac{v\ (\textit{rebound})}{v\ (\textit{impact})} \tag{15}$$

The resulting experimental values for e are given in Table 6. The wide variations in results for the irregularly-shaped objects show that e is sensitive to impact attitude.

Table 6. Experimental Values for Coefficient of Restitution

			Coef. of Restitution	
Item	Dimensions (inches)	Weight (oz)	Hard Surface	Soft Surface
basketball	9" diameter	20	0.66	0.61
softball	3.5" diameter	6.4	0.60	0.08
tennis ball	2.5" diameter	2.0	0.72	0.52
wood block	1.5" x 1.5" x 3.2"	1.5	0.21 - 0.50	0.24 - 0.33
steel bolt and nut	4.2" long, 0.25" diam.	1.7	0.30 - 0.43	0.00 - 0.20
thin steel cup	1" deep x 2.75" diam.	1.8	0.26 - 0.48	0.15 - 0.24

At best, the results in Table 6 serve only as a rough guide in estimating coefficients of restitution for low-velocity impacts of space-vehicle debris. It seems apparent that the hard-surface values should be chosen well below those computed for the three balls, yet somewhat higher than the experimental values obtained for other items, since some space-vehicle debris could well be more resilient. If any proof is needed, the drop tests also show that the hard-surface coefficients are generally well above those for soft surfaces, with maximum values about twice those measured for soft surfaces. Since values chosen for e will be applied to widely diverse components and debris, agonizing over the values to be selected is not justified. Accordingly, based on the data presented

in Sections 7.2, 7.3, and 7.4, RTI has assumed that the hard-surface and soft-surface coefficients of restitution for low-impact-velocity debris are 0.5 and 0.25, respectively.

7.5 Assumed Coefficient of Restitution and Bounce Results

Since the coefficient of restitution e depends – among other things – on impact velocity[6] after some minimum velocity is exceeded, the assumption has been made that e varies inversely with the logarithm of impact velocity V_{IP} beyond this minimum value. The assumed relationships are shown in Fig. 4, one for impacts on hard surfaces, the other for impacts on soft surfaces. For hard surfaces, e has a constant value of 0.50 for V_{IP} less than or equal to 40 feet per second, and thereafter decreases linearly (in the log domain) to zero for V_{IP} = 300 feet per second. In equation form,

$$\begin{aligned} e &= 0.50 && (V_{IP} \le 40) \\ e &= 1.415 - 0.5714 \log_{10}(V_{IP}) && (40 < V_{IP} \le 300) \end{aligned} \qquad (16)$$

For soft surfaces, e has a constant value of 0.25 for V_{IP} less than 60 feet per second, and thereafter decreases to zero for V_{IP} = 200 feet per second. In equation form,

$$\begin{aligned} e &= 0.25 && (V_{IP} \le 60) \\ e &= 1.100 - 0.4781 \log_{10}(V_{IP}) && (60 < V_{IP} \le 200) \end{aligned} \qquad (17)$$

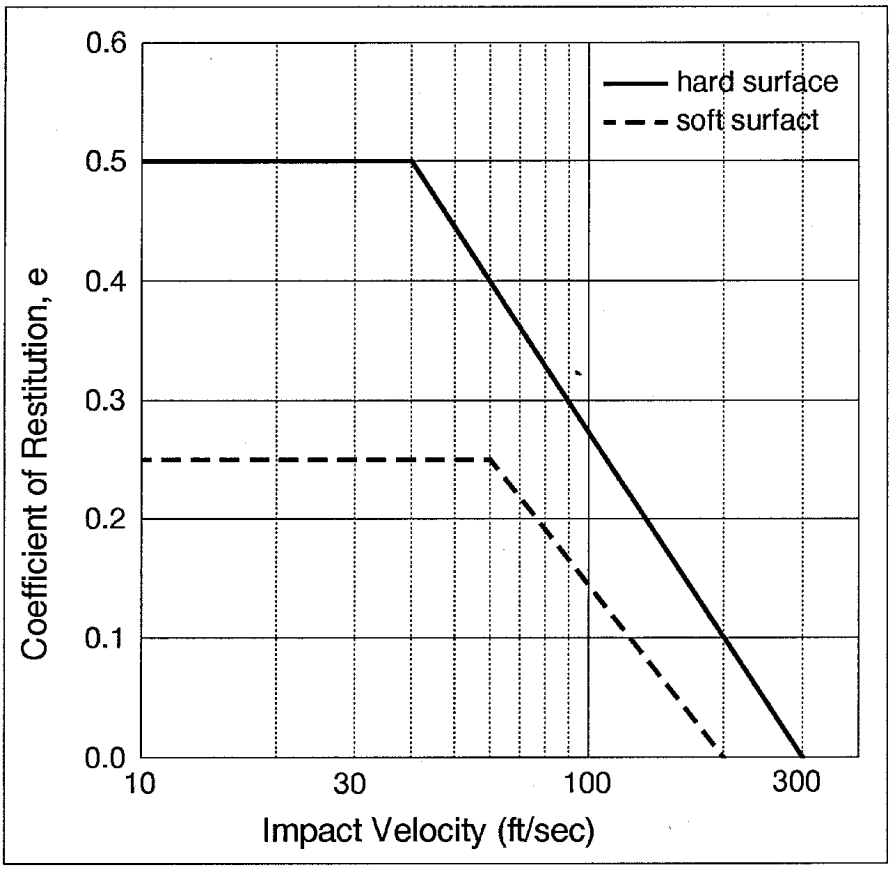

Figure 4. Coefficients of Restitution for Bounce

Although no real justification can be provided, the basis for the assumed relationships in Fig. 4 is as follows:

(a) They are consistent with the notion that, beyond some relatively small impact velocity, e should decrease with velocity, since the energy consumed in deforming both the impacting and impacted bodies increases with velocity. For high values of e, relatively little energy is lost in deforming either body.

(b) For impacts on hard surfaces at small impact velocities (≤40 ft/sec), e has a value of 0.50, which is well below the values obtained experimentally for three types of balls, and below the value given in Ref. [5] for iron impacting on iron. (Available handbooks do not provide coefficients for impacts of metallic objects on concrete, rock, or sand.) Smaller values of e are assigned for soft surfaces, since surely the bounce on soft surfaces would be less.

(c) For space-vehicle debris, it seems apparent that e will never decrease with velocity in a predictable or consistent manner. Since a linear decrease leads to unreasonable bounce heights for high impact velocities, some more rapidly decreasing function is needed. Logarithmic functions produce (seemingly)

reasonable bounce heights for the assumed range of impact velocities. Since the relationship between e and velocity involves considerable speculation, the assumption of a log function seems as good as any other.

(d) The assumed relationships establish upper limits for impact velocities that can produce bounce. Beyond these limits, the body is assumed to break apart or bury itself, thus producing splatter and no bounce. A smaller limiting velocity is chosen for soft surfaces than for hard, since the kinetic energy for a soft-surface impact is more likely to be consumed by the body in producing a crater and in burrowing into the ground.

For values of V_{IP} above 300 feet per second (hard surfaces) or 200 feet per second (soft surfaces) where e = 0, breakup of the body upon impact or digging into the ground precludes bounce as defined here. The fragments of an impacting body that do in fact bounce are considered to be splatter fragments. Casualty areas for those fragments are evaluated as described later in Section 8.

Using the assumed relationships for e and a mean annual wind speed for Cape Canaveral of 11.5 ft/sec[7], bounce distances and heights were calculated for terminal velocities V_T of impacting components having various values of β. Results are given in Table 7 for both hard and soft surfaces.

Table 7. Bounce Distances and Heights

β (lbs/ft^2)	V_T (ft/sec)	e		Horizontal Bounce Distance (ft)		Bounce Height (ft)	
		Hard	Soft	Hard	Soft	Hard	Soft
0.2	13.2	0.500	0.250	2.36	0.59	0.68	0.17
0.5	20.9	0.500	0.250	3.74	0.93	1.70	0.43
1.0	29.6	0.500	0.250	5.29	1.32	3.40	0.85
2.0	41.8	0.479	0.250	6.87	1.87	6.25	1.70
5.0	66.2	0.371	0.227	6.51	2.43	9.36	3.49
10.	93.6	0.287	0.156	5.50	1.63	11.19	3.31
20.	132.3	0.202	0.085	3.85	0.68	11.08	1.96
25.	147.9	0.174	0.062	3.21	0.40	10.33	1.30
30.	162.0	0.152	0.043	2.67	0.21	9.40	0.76
40.	187.1	0.116	0.013	1.81	0.02	7.35	0.10
50.	209.2	0.089	0.000	1.18	0.00	5.35	0.00
60.	229.2	0.066	0.000	0.72	0.00	3.57	0.00
80.	264.6	0.030	0.000	0.18	0.00	1.01	0.00
100.	295.9	0.003	0.000	0.00	0.00	0.01	0.00

7.6 Casualty Area for Low Bounce

If the vertical component of rebound velocity is less than $(2gh_p)^{1/2}$ where h_p is the height of a person, the bouncing fragment will not rise above h_p. In this case, the additional casualty area for bounce is

$$A_c(\text{bounce}) = 2(r_f + r_p)d_b \tag{18}$$

where r_f is the equivalent radius of the impacting fragment, r_p is the radius of a person, and d_b is computed from Eq. (11). It can be seen that Eq. (18) is the same as Eq. (6) except d_b has replaced d_s.

7.7 Casualty Area for High Bounce

For most fragments except possibly early in flight, the path angle of the velocity vector at impact (relative to the horizontal) is well above 70°. As a result, the height of bounce can be considerably greater than the horizontal bounce distance. During the period that the bouncing piece is above height h_p, the vulnerable individual may be justifiably excited although not actually hit. The casualty area computed from Eq. (18) must be modified to account for this.

7.7.1 High and Long Bounce

Consider first the case depicted in Fig. 5, where the bounce distance is so large that the position of the piece at height h_p on the way up does not overlap the position of the piece at height h_p on the way down. From left to right, four positions of the bouncing fragment are shown in plan view where, in all cases, the fragment radius r_f has been augmented by the radius of a person r_p:

(1) Position at first impact
(2) Position during first upward bounce when fragment has risen to height h_p
(3) Position during first bounce when fragment has descended to height h_p
(4) Position of fragment at second impact.

As evident from the figure, a circularized flat piece has been postulated with the flat surface parallel to the ground throughout the bounce.

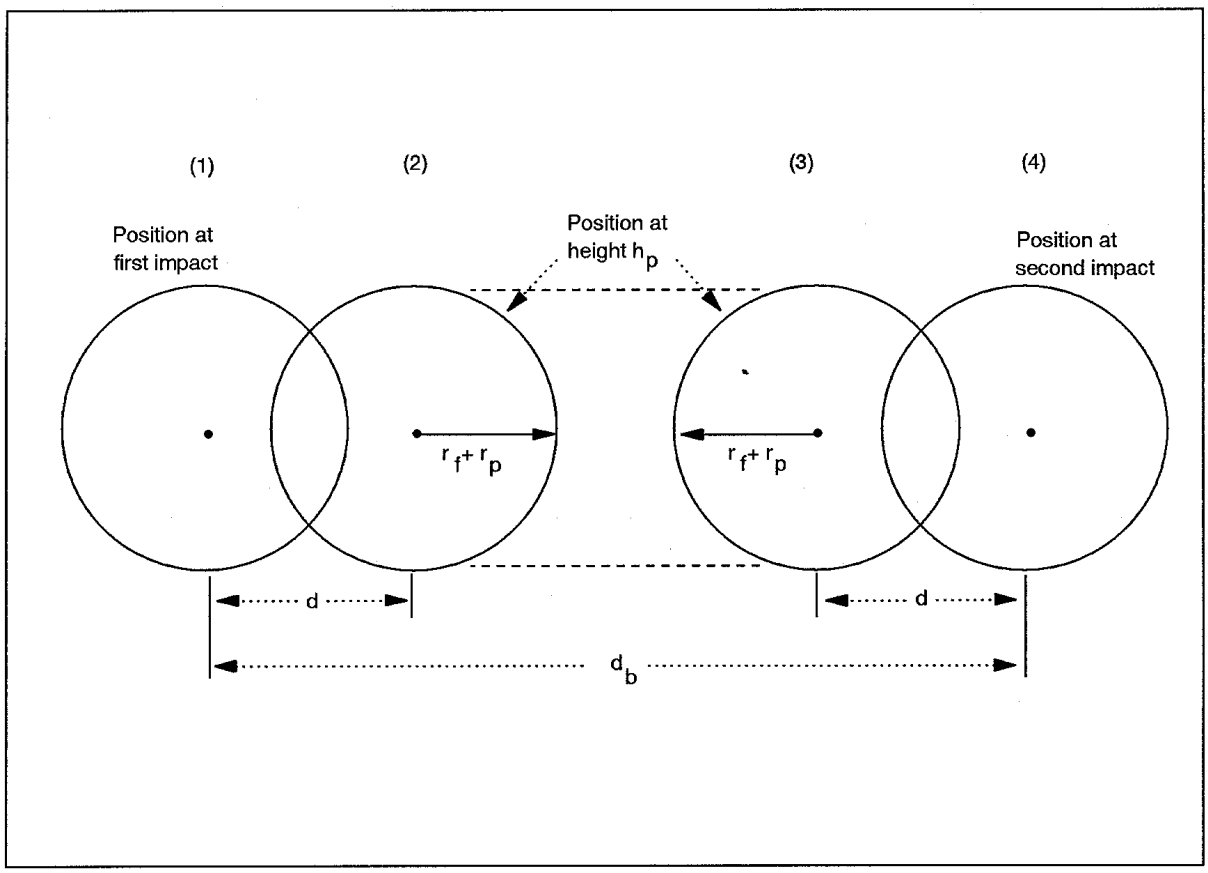

Figure 5. Plan View for Long-Bounce Fragment

From Fig. 5 it can be seen that

$$d_b \geq d + (r_f + r_p) + (r_f + r_p) + d = 2(d + r_f + r_p) \tag{19}$$

where d_b is the total bounce distance on the first bounce, and d is the horizontal distance traveled while the fragment rises to height h_p, and again while it falls from height h_p. The time to reach height h_p during the first bounce can be calculated from the equation

$$t_{h_p} = \frac{v_r \sin\phi + \sqrt{(v_r \sin\phi)^2 - 2gh_p}}{g} \tag{20}$$

where v_r is computed from Eq. (7) and ϕ from Eq. (8). (If the radicand in Eq. (20) is negative, the bouncing fragment does not reach height h_p.) The distance d in Fig. 5 is calculated from

$$d = t_{h_p} v_{hr} \tag{21}$$

where v_{hr} is determined from the second of Eqs. (9).

For this case (high and long bounce), the casualty area due to bounce becomes

$$\begin{aligned} A_c(\text{bounce}) &= \left[2\left(r_f + r_p\right)d\right] + \left[2\left(r_f + r_p\right)d + \pi\left(r_f + r_p\right)^2\right] \\ &= 4\,d\left(r_f + r_p\right) + \pi\left(r_f + r_p\right)^2 \end{aligned} \tag{22}$$

As in the case of slide, the area of the fragment at first impact must not be included in Eq. (22), since this area has already been accounted for in the basic casualty area given by Eq. (4). Since, in fact, the first bracketed term in Eq. (22) does include half the area of the fragment at impact, the leading half of the fragment at height h_p on the way up is omitted from the equation to compensate for this.

7.7.2 High and Short Bounce

If the bounce distance is not so large, the up and down positions of the bouncing piece at height h_p may overlap. In this case,

$$d_b < 2\left(d + r_f + r_p\right) \tag{23}$$

and elimination of the duplicated area becomes a bit messy. Consider Fig. 6 where the solid-line circles indicate the positions of the augmented fragment during the first bounce at height h_p on the way up and again at h_p on the way down. The distance between these two positions is $(d_b - 2d)$, where d_b and d are as defined previously for Fig. 5.

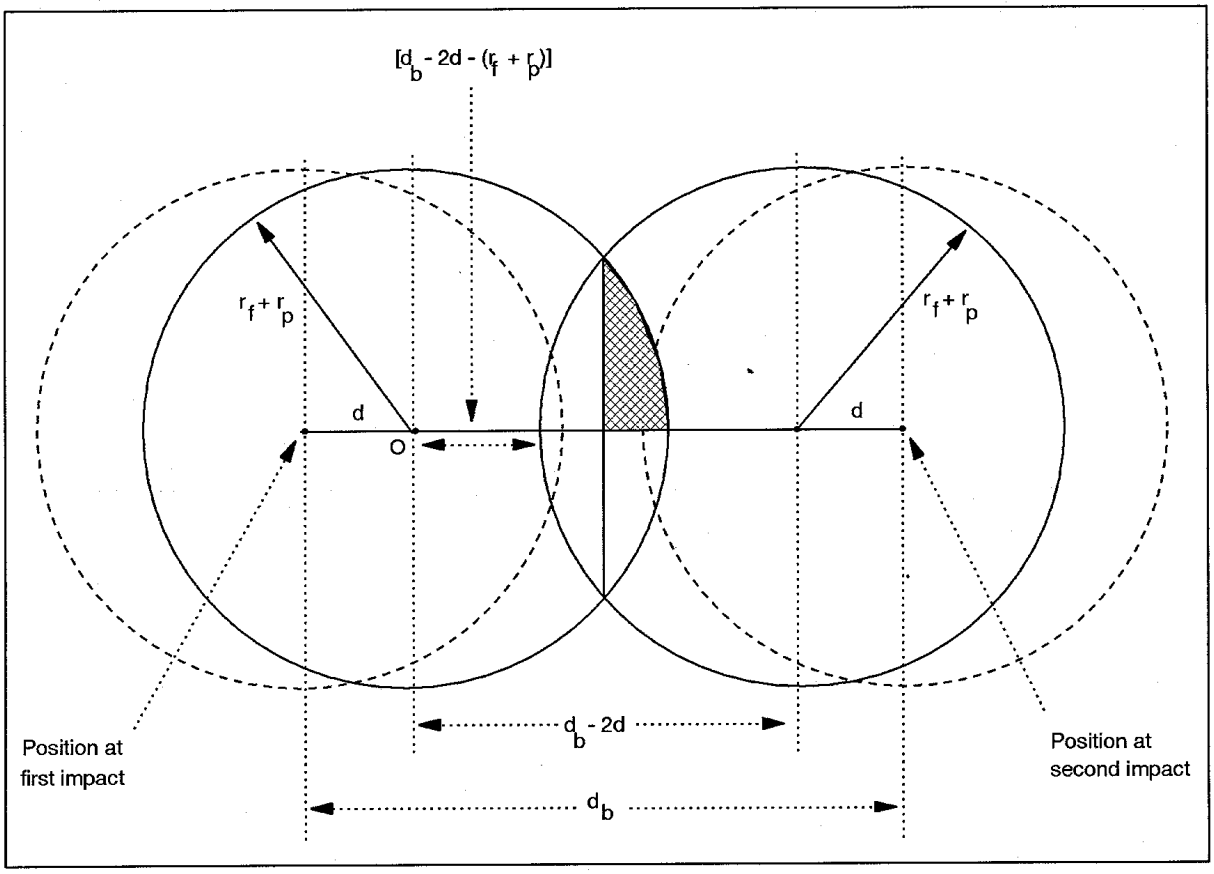

Figure 6. Plan View for Short-Bounce Fragment

In summing the component areas that comprise A_c(bounce), the area A formed by the intersection of the two solid-line circles must not be included twice. It can be found by multiplying the shaded area shown in the figure by four. If the origin of the orthogonal X-Y coordinate system is chosen at O with the X-axis along the centerline of the bouncing piece, the equation of the left-hand circle is $x^2 + y^2 = r^2$. Then

$$A = 4 \int_a^r (r^2 - x^2)^{1/2} dx \tag{24}$$

where $a = (d_b - 2d)/2$ and $r = (r_f + r_p)$. Performing the integration and simplifying,

$$A = \pi r^2 - 2a\sqrt{r^2 - a^2} - 2r^2 \sin^{-1}\left(\frac{a}{r}\right) \tag{25}$$

After evaluating A, the casualty area can be found for the high and short bounce, where $d_b < 2(d + r_f + r_p)$. In summing the component areas shown in Fig. 6 to arrive at an

equation for A_c(bounce), overlapping areas must not be counted twice. The left half of the fragment at first impact is excluded, since it has already been included in the basic casualty area from Eq. (4); and the right half of the fragment at first impact is cancelled by omitting the right half of the fragment at second impact. If the duplicated area A is then subtracted, the equation for A_c(bounce) becomes

$$\begin{aligned} A_c(\text{bounce}) &= 2(r_f + r_p)d + \pi(r_f + r_p)^2 + 2(r_f + r_p)d - A \\ &= 4d(r_f + r_p) + \pi(r_f + r_p)^2 - A \end{aligned} \tag{26}$$

7.8 Multiple Bounces

The information presented so far in Section 7 does not address the possibility of multiple bounces. In view of the potential error in estimating coefficients of restitution for irregular components impacting in unknown attitudes on uncertain surfaces, consideration of multiple bounces may seem like "overkill".

From Table 7 the highest first bounce on a hard surface occurs for a piece having a ballistic coefficient of 10 lbs/ft^2 and a terminal velocity of 93.6 ft/sec. The data in Table 8 have been computed to show, theoretically at least, bounce heights and distances for the first five bounces of that object. Although, in theory, bouncing would continue forever, it seems apparent that a practical limit would be reached after one or two bounces.

Table 8. Multiple Bounce Heights and Distances on Hard Surfaces

	β = 10 lbs/ft^2, V_T = 93.6 ft/sec						
Bounce No.	Vertical impact velocity (ft/sec)	Horiz. impact velocity (ft/sec)	Total impact velocity (ft/sec)	Coef. of resti. e	Total rebound velocity (ft/sec)	Bounce height (ft)	Bounce distance (ft)
1	93.6	11.5	94.3	0.287	27.0	11.19	5.50
2	26.8	3.3	27.0	0.500	13.5	2.80	1.38
3	13.4	1.6	13.5	0.500	6.8	0.70	0.34
4	6.7	0.8	6.8	0.500	3.4	0.17	0.09
5	3.4	0.4	3.4	0.500	1.7	0.04	0.02

For this worst-case example from Table 8, the second-bounce height is only 2.8 feet, well below the height of a person. Thus, in estimating the additional casualty area caused by any bounce after the first, low-bounce procedures apply. However, as stated earlier

in the section, consideration of multiple bounces in casualty-area evaluation seems to be an unjustifiable complexity in view of the uncertainty in the overall process. Consequently, RTI excludes multiple-bounce considerations in estimating effective casualty areas for input to program DAMP.

7.9 Unequal Impact and Rebound Angles

In developing equations for A_c(bounce), the assumption has been made that the impact and rebound angles are equal. As observed from the drop tests of the irregularly-shaped objects, these angles were generally quite different for low-velocity impacts, with the rebound angle varying between 0° and 90°, while the impact angle was kept as close as possible to 90°. Various rebound angles are probably caused by irregularities in the impacting and impacted bodies and by rotation of the impacting body. This suggests that the procedures set forth in Sections 7.6 and 7.7 should be adjusted to account for the fact that the impact and rebound angles may not be equal.

7.9.1 Density Function for Rebound Angle

Repeated trials with irregular objects seemed to show that any rebound angle between 0° and 90° was possible when the impact angle was near 90°, although higher rebound angles occurred more frequently. As the impact velocity was increased by forceful throws, the higher rebound angles seemed to become more likely. Although the tests were too crude to be conclusive, it was inferred that low or intermediate impact angles will generally produce low or intermediate rebound angles, with no rebound angle (even backwards) being impossible. Although considerable speculation is involved, RTI has assumed from these simple experiments that for impact angles of 90° and 0° the density functions for the rebound angle are as shown in Fig. 7. It can be seen that the rebound-angle density function for a 90° impact angle (ϕ_I = 90°) increases linearly from 0° to 90°, while the density function for ϕ_I = 0° does the reverse.

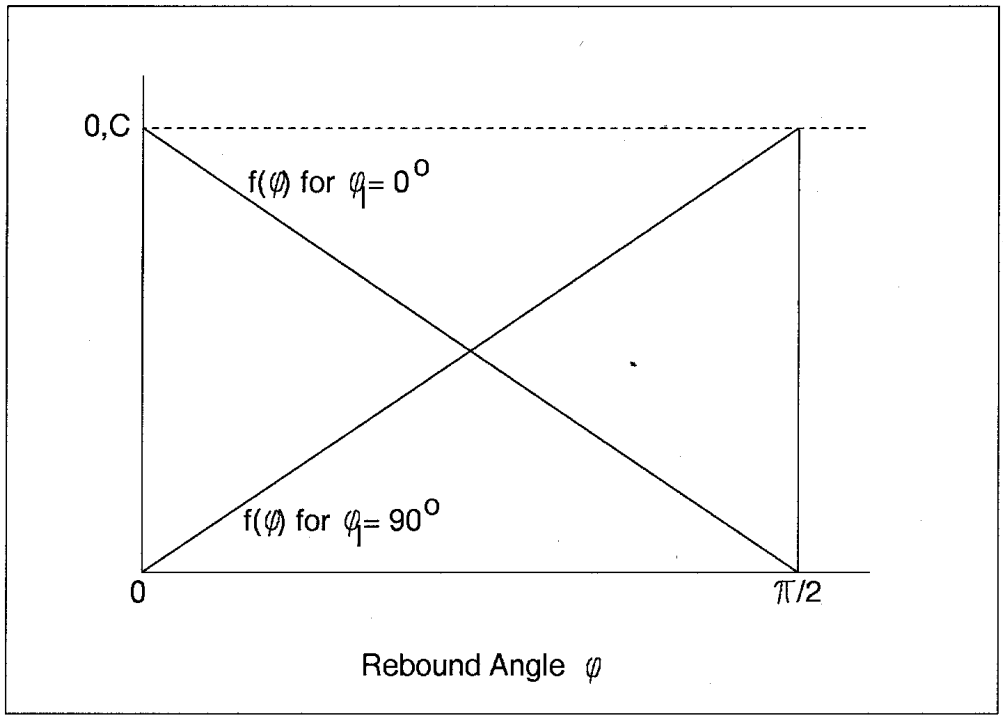

Figure 7. Rebound-Angle Density Function for Impact Angles of 90° and 0°

Since the area under the curve must be unity, the constant $C = 4/\pi$, and the density-function equations for rebound angle ϕ become

$$\begin{aligned} \textit{Impact angle } \phi_I = 90°: \quad f(\phi) &= \frac{8}{\pi^2}\phi \\ \textit{Impact angle } \phi_I = 0°: \quad f(\phi) &= \frac{4}{\pi} - \frac{8}{\pi^2}\phi \end{aligned} \tag{27}$$

The further assumption is made that the rebound velocity can be calculated from Eq. (15) for any rebound angle, i.e., v(rebound) = e v(impact).

The density-function curves in Fig. 7 for impact angles of 90° and 0° served as a basis for postulating the density-function curve shown in Fig. 8 for any intermediate impact angle ϕ_I. It can be seen that the most likely rebound angle is equal to the impact angle, while the changes in probability for rebound angles greater than and less than the impact angle are at the same constant rates assumed for the impact density functions for 0° and 90°.

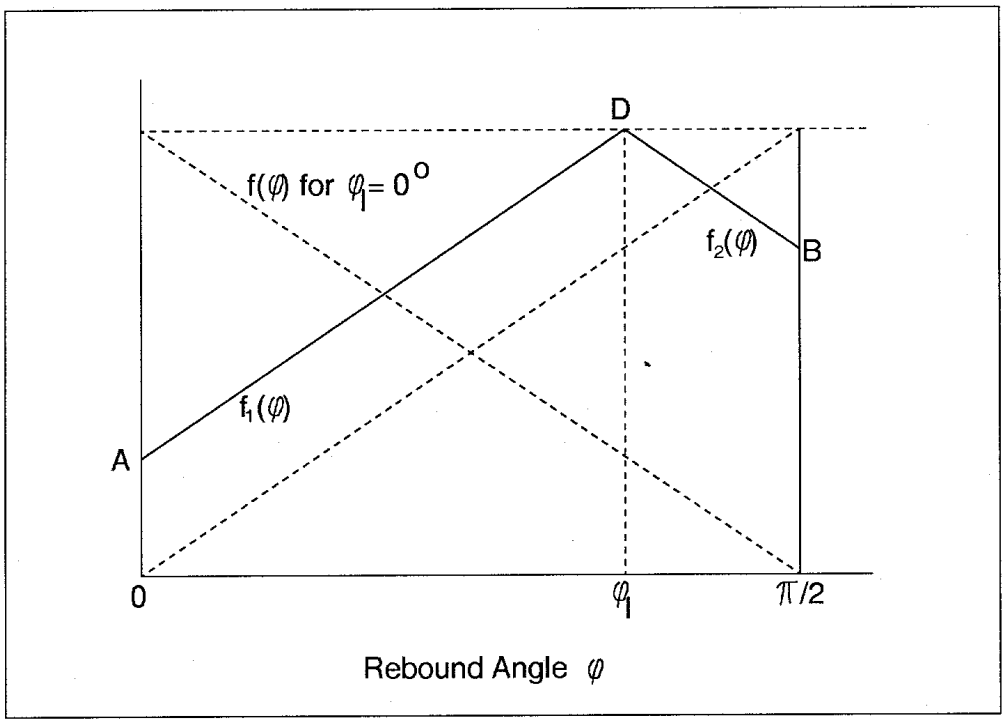

Figure 8. Rebound-Angle Density Function for Intermediate Impact Angle

For the assumed density function in Fig. 8, the slope of the line $f_1(\phi)$ from A to D is $8/\pi^2$, while the slope of $f_2(\phi)$ from D to B is $-8/\pi^2$. Knowing that the area under the density-function curve must be unity, with some algebraic manipulation the following results can be obtained:

$$B = \frac{2}{\pi} - \frac{8}{\pi^3}\left[\phi_I^2 + \left(\frac{\pi}{2} - \phi_I\right)^2 + 2\phi_I\left(\frac{\pi}{2} - 2\phi_I\right)\right]$$

$$D = B + \frac{8\left(\frac{\pi}{2} - \phi_I\right)}{\pi^2} \tag{28}$$

and

$$f_1(\phi) = D + \frac{8}{\pi^2}\left(\phi - \phi_I\right)$$

$$f_2(\phi) = D - \frac{8}{\pi^2}\left(\phi - \phi_I\right) \tag{29}$$

7.9.2 Computation of Casualty Area for Variable Rebound Angle

So that all values of rebound angle ϕ between $\pi/2$ and zero are considered in calculating the casualty area due to bounce, the range of values for ϕ is divided into n equal intervals, with the midpoint of each interval calculated from

$$\phi_i = \left(\frac{\pi/2}{n}\right)\left(i - \frac{1}{2}\right), \quad i=1,2,\cdots,n \tag{30}$$

For an assumed value of ϕ_i, the horizontal and vertical components of rebound velocity are first computed, then the distance and height of bounce. If the bounce height is less than h_p, $A_c(\text{bounce})_i$ is determined from Eq. (18). If the bounce height is greater than h_p, a test is made using Eq. (19) to determine whether the bounce is "high and long" or "high and short". For the first case, $A_c(\text{bounce})_i$ is found from Eq. (22); for the latter, from Eq. (26).

The value of $A_c(\text{bounce})_i$ must now be weighted by the probability that the rebound angle lies in the interval with midpoint ϕ_i. Since the density-function segments are linear, this probability p_i can be found by multiplying the height of the function at ϕ_i by the interval width. Thus

$$p_i = f(\phi_i)\frac{\pi}{2n} \tag{31}$$

The same procedure is followed for each assumed value for ϕ_i. The casualty area for bounce is then obtained from

$$A_c(\textit{bounce}) = \sum_{i=1}^{n} p_i A_c(\textit{bounce})_i, \quad i = 1,2,\cdots,n \tag{32}$$

7.9.3 Casualty-Area Example

The procedures set forth in Section 7.9.2 for variable rebound angles were applied with n = 9 for a piece impacting at an angle of 80° (relative to the horizontal) and a speed of 94.3 ft/sec. The resulting casualty-area computations are summarized in Table 9. The final result of 35.9 ft^2 for A_c(bounce) is significantly greater than the value (15.6 ft^2) obtained when assuming equal incident and rebound angles of 80°.

Table 9. Bounce Casualty Area Using Variable Rebound Angles

Interval i	ϕ_i (deg)	Bounce height (ft)	Casualty distance (ft)	$A_c(\text{bounce})_i$ (ft^2)	p_i	Weighted $A_c(\text{bounce})_i$ (ft^2)
1	5	0.1	3.9	12.3	0.015	0.186
2	15	0.8	11.4	35.5	0.040	1.414
3	25	2.0	17.4	54.5	0.064	3.511
4	35	3.7	21.4	66.8	0.089	5.957
5	45	5.7	22.7	71.1	0.114	8.094
6	55	7.6	14.0	43.7	0.139	6.048
7	65	9.3	9.5	29.6	0.163	4.832
8	75	10.6	6.3	19.8	0.188	3.724
9	85	11.3	3.7	11.1	0.188	2.091
Total	-	-	-	-	1.000	35.858

The nine intervals shown in Table 9 were used to illustrate the procedure for variable rebound angle. When using 45 intervals, the final result for $A_c(\text{bounce})$ is 35.4 ft^2.

8. Splattering and Cratering

If an inert vehicle piece or component impacts in an open area, piece fragments or chunks of the impacted surface may be forcefully projected away from the periphery of the falling piece. Such projected fragments may pose a significant risk to people nearby. For high-velocity impacts on hard surfaces such as rock, concrete, and blacktop, piece fragments and surface chunks may be thrown outward considerable distances. For impacts on soft surfaces such as lawns, fields, roadsides, and sandy beaches, splattering and cratering hazards will be considerably reduced. For low-velocity impacts, the kinetic energy may be insufficient to produce either splattering or cratering, although the possibility of bounce or skid still exists.

Although some experimental data pertaining to cratering and fragment projection from explosive charges are available in the literature, little or no similar data exist for inert-piece impacts, insofar as can be determined. Thus, in modeling such events, the analyst is largely left to his own resourcefulness and imagination. Claims of rigor and precision cannot be made for such modeling. Still, splattering and cratering phenomena exist in the real world, so even a speculative model should be superior to no model at all.

In estimating casualty area due to splatter, both hard and soft surfaces are considered. Except for the functions used to define the maximum splatter range and the number of splatter fragments, the procedures and equations for the two surfaces are identical. In making risk calculations for people in the open, the type of surface on which each person or group of people is located must be specified. If the type is unknown or not indicated, the assumption is made that the surface is hard.

8.1 Basic Assumptions

With the above caveats in mind, the following basic assumptions have been made in modeling splattering and cratering effects from inert impacts. Specific assumptions about the number of splatter fragments produced, and the maximum range to which fragments are projected, are provided later:

a. Splatter fragments are thrown radially outward from the boundary of the impacting piece, with all directions being equally likely.

b. Impacting vehicle pieces and projected fragments can be approximated by circles of equivalent cross-sectional areas.

c. A person can be represented by a right circular cylinder having a height of h_p feet and a radius of r_p feet.

d. A person in the open will be hit by a splatter fragment if two conditions are satisfied:

(1) the person is located along the radial line of travel of the projected fragment,
(2) the person is within the range interval traversed by the fragment when the fragment is within h_p feet of the ground.

8.2 Splatter-Range Density Function

As a first step in deriving an effective casualty area for projected splatter fragments, a splatter-range density function will be established. In deriving the function, the assumption is made that the impact probability for each projected fragment decreases linearly from the point of piece impact out to some maximum impact range r_{max}, beyond which the probability is zero. (The rationale for this assumption and its consequences are given in Section 4.3.2 of an earlier RTI report[8].) The term 'maximum impact range', as used here, means the maximum hazardous distance (rather than the maximum possible distance) from the edge of the impacting piece. Although a fragment may roll or bounce somewhat farther than this, it would not be considered hazardous beyond this range since its velocity would be low and dropping to zero. The assumed function is shown in Fig. 9, where r_{max} is the maximum hazardous distance measured from the edge of the impacting piece, and A is a constant to be determined. Methods for estimating numerical values for r_{max} are given in Section 8.6.

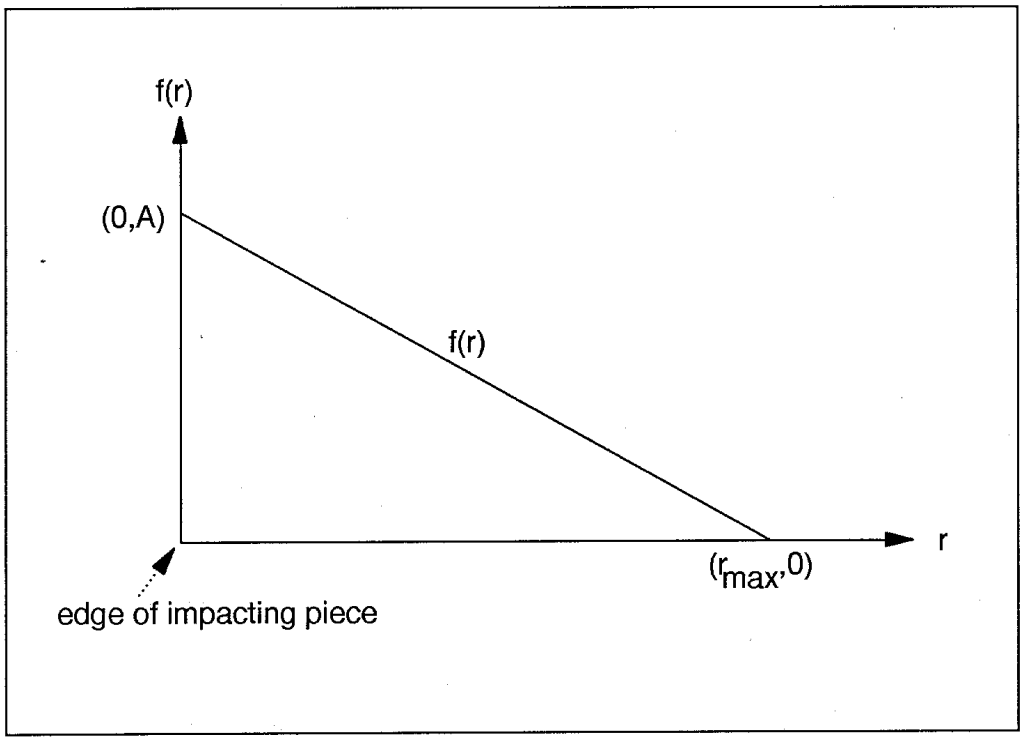

Figure 9. Splatter-Range Density Function

Since the area under f(r) must be unity, the constant $A = 2/r_{max}$, and

$$f(r) = \frac{2}{r_{max}^2}(r_{max} - r) \tag{33}$$

8.3 Casualty Area for Fixed Splatter Range With No Overflight

Even if a splatter fragment is projected directly toward a person with sufficient velocity to reach or impact beyond the person, he or she would not be hit if the fragment passes overhead. For the moment, however, the possibility of overflight will be neglected. Instead, the simplifying assumption is made that a fragment projected in the proper direction with sufficient range will score a hit, with this latter condition being equivalent to the assumption that the fragment trajectory never rises above h_p feet. The effective (or average) casualty area for the fragment will now be evaluated for this case. Figure 10 is a ground-plane depiction of a projected fragment that impacts at distance r from the origin (edge of impacting piece).

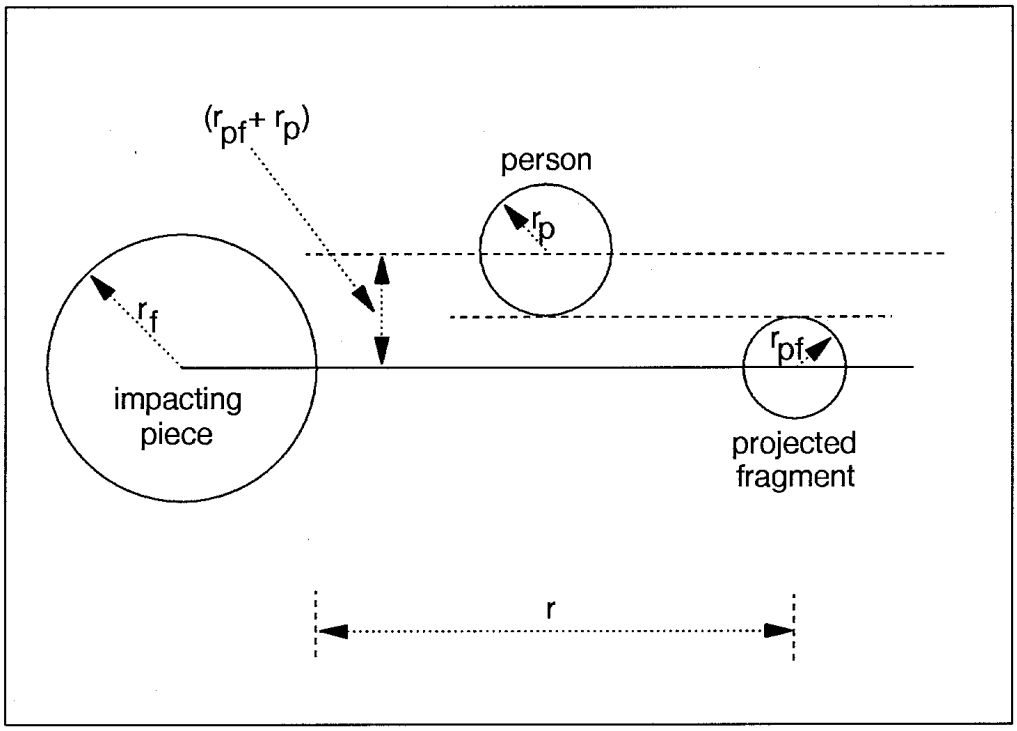

Figure 10. Casualty Area for Splatter Fragment

It is apparent from the figure that a person located on either side of the center line of travel of the projected fragment within a distance of $(r_{pf} + r_p)$ will be hit. For this particular impact range r, the effective casualty area becomes approximately

$$A_c(\text{fixed splatter range}) \approx 2\left(r_{pf} + r_p\right)\left(r - r_p\right) + \frac{\pi}{2}\left(r_{pf} + r_p\right)^2 \qquad (34)$$

In the second pair of parentheses, r_p is subtracted from r to avoid duplication of an area already accounted for by the second term in Eq. (4). Since Eq. (34) applies for a single fixed splatter range r, it serves only to introduce basic concepts. The calculation of effective casualty area must account for the fact that the projected fragment can impact anywhere out to range r_{max} in accordance with the density function shown in Fig. 9.

8.4 Casualty Area for All Range Intervals With No Overflight

Now consider Fig. 11 where the distance r_{max} has been divided into n equal intervals, one such interval being shown as shaded in the figure. The interval width w is simply r_{max}/n.

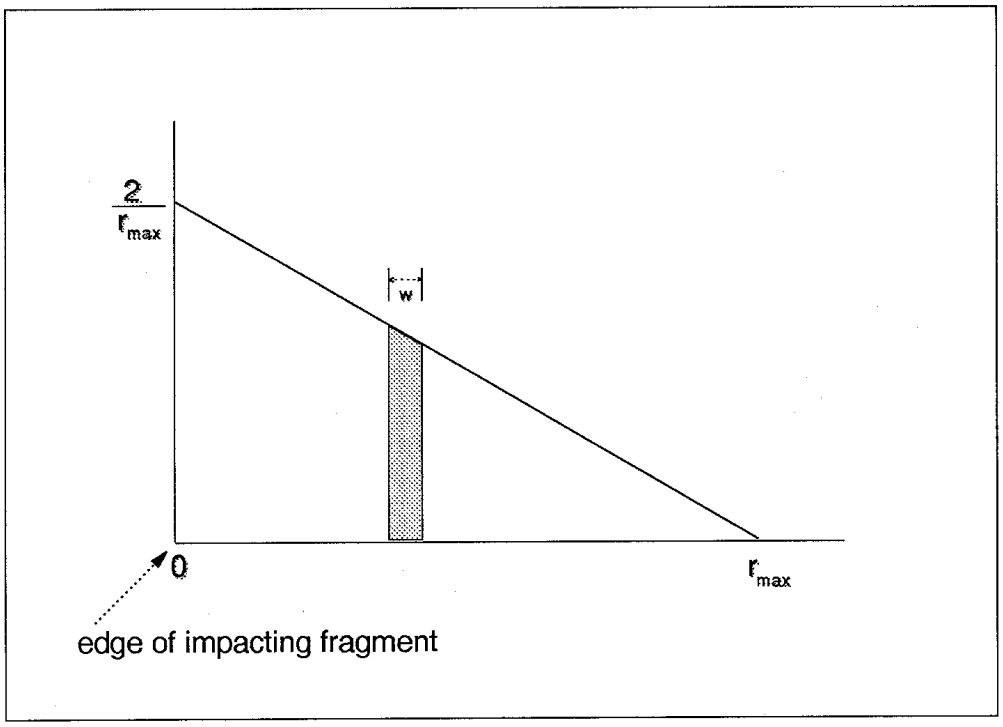

Figure 11. Splatter-Range Density-Function Interval

The distance, r_i, from the origin to the midpoint of interval i is

$$r_i = \left(\frac{r_{max}}{n}\right)\left(i - \frac{1}{2}\right), \; i = 1, \cdots, n \qquad (35)$$

The probability that the center of the splatter fragment impacts in interval i can be found by integrating the density function f(r) over the interval. Since f(r) is a straight line, the same result is obtained by multiplying the height of the density function at $r = r_i$ by the interval width. Using Eq. (33),

$$\text{Prob}\left(r_i\right) = \frac{2\left(r_{max} - r_i\right)}{r_{max}^2} w \tag{36}$$

For the i^{th} interval, the effective casualty area is obtained by multiplying the probability of impacting in the interval [Eq. (36)] by the area swept out by the projected fragment [Eq. (34)]. The total effective area for the fragment is the sum for all such intervals i. With the restriction that the trajectory for the projected fragment does not rise above h_p feet, the conditional effective casualty area for a single projected fragment can thus be written as follows:

$$\begin{aligned} A_c\,(\text{no overflight}) &= \sum_{i=1}^{n}\left[\frac{2w\left(r_{max} - r_i\right)}{r_{max}^2}\right]\left[2\left(r_{pf} + r_p\right)\left(r_i - r_p\right) + \frac{\pi}{2}\left(r_{pf} + r_p\right)^2\right] \\ &= \frac{4w\left(r_{pf} + r_p\right)}{r_{max}^2}\sum_{i=1}^{n}\left(r_{max} - r_i\right)\left[\left(r_i - r_p\right) + \frac{\pi}{4}\left(r_{pf} + r_p\right)\right] \end{aligned} \tag{37}$$

8.5 Elimination of No-Overflight Restriction

The restriction on trajectory height will now be removed to allow for the possibility that the projected fragment may overfly a vulnerable individual. Some speculation is involved since there is no way to know what trajectory a fragment flies in reaching a particular impact range. In view of this uncertainty, corrections to the conditional effective casualty area are made using vacuum calculations and a flat, non-rotating, constant-gravity earth.

Figure 12 depicts the trajectory of a flat circular fragment that is projected above height h_p before impacting at distance r_i from the origin. Throughout flight the fragment plane is assumed to be horizontal.

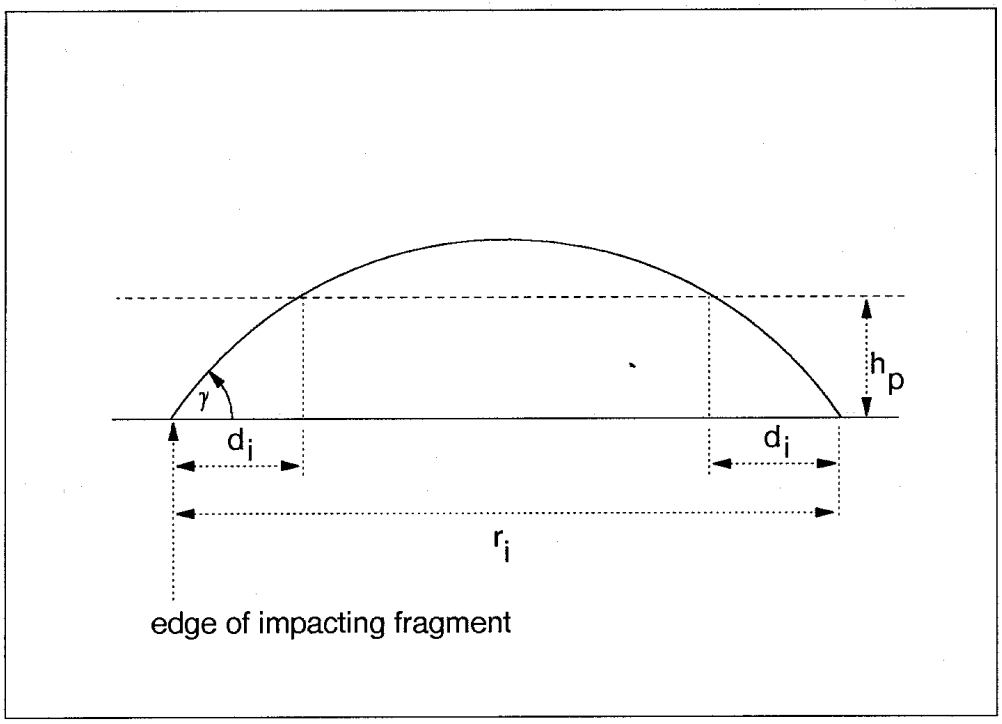

Figure 12. Fragment Projected Above Height of a Person

As shown in the figure, the fragment is below h_p feet and thus hazardous during the first and last d_i feet of horizontal travel rather than for the entire distance r_i. (Note: for vacuum calculations, the two distances labeled d_i are equal.) Thus, Eq. (37) must be revised to reflect this fact. If the projection angle γ is known, the projection velocity v_o needed to reach range r_i can be calculated by

$$v_o = \sqrt{\frac{g\, r_i}{\sin(2\gamma)}} \tag{38}$$

where g is the gravitational acceleration (32.174 ft/sec^2). The time to reach height h_p can be computed from the equation

$$t_h = \frac{v_o \sin\gamma - \sqrt{(v_o \sin\gamma)^2 - 2gh_p}}{g} \tag{39}$$

The distance d_i is then calculated by

$$d_i = t_h v_o \cos\gamma \tag{40}$$

The time to reach a height of h_p can be computed from Eq. (39) only if the trajectory rises to or above that height. When the apogee is less than h_p, the term under the square root sign in Eq. (39) is negative, Eq. (40) is bypassed, and d_i is set equal to $r_i/2$.

To carry out the calculations indicated in Eqs. (38) through (40), a value of γ is needed. Rather than select an arbitrary value for γ, the following procedure is used to compute d_i for each interval i of width w:

(1) For the maximum hazardous projection range r_{max}, a projection velocity v_{max} is computed from Eq. (38) with $\gamma = 45°$.

(2) A value of r_i is determined from Eq. (35).

(3) The minimum projection velocity v_{min} to reach range r_i is computed from Eq. (38) with $\gamma = 45°$.

(4) The velocity interval from v_{min} to v_{max} is divided into m equal sub-intervals. For each of the m+1 velocities v_j, the two initial path angles that produce impact range r_i are computed from Eqs. (41) and (42), where Eq. (41) is obtained by solving Eq. (38) for γ.

$$\gamma_j(\text{smaller}) = \frac{1}{2}\sin^{-1}\left(\frac{g r_i}{v_j^2}\right) \quad (j = 1,2,\cdots,m+1) \tag{41}$$

$$\gamma_j(\text{larger}) = 90 - \gamma_j(\text{smaller}) \quad (j = 1,2,\cdots,m+1) \tag{42}$$

(5) For each of the (m + 1) velocities and corresponding pairs of path angles, values of d_i are computed using Eqs. (39) and (40).

(6) Assuming that all velocities and their corresponding pairs of path angles are equally likely, a mean value of d_i is computed from the set of (2m + 1) values determined in step (5).

Steps (2) through (6) are repeated for all values of i.

After a mean value of d_i has been computed for the midpoint of each range interval, Eq. (37) can be adjusted to eliminate the portion of the ground area swept out while the fragment altitude is above h_p feet. This becomes a little messy because the horizontal distance traveled while the fragment is below h_p must be reduced by the radius of a person r_p. This avoids duplication of the casualty area that has already been included in the basic casualty area of the impacting fragment [see Fig. 2 and Eq. (4)]. The adjustment to Eqs. (37) is done by replacing $(r_i - r_p)$ by a quantity Q_i, which is the horizontal distance traveled by the projected fragment when it is simultaneously farther

from the origin than r_p and also below height h_p. With this replacement, Eqs. (37) become

$$A_c\,(\text{splatter/piece}) = \sum_{i=1}^{n}\left[\frac{2w\left(r_{max} - r_i\right)}{r_{max}^2}\right]\left[2\left(r_{pf} + r_p\right)\left(Q_i\right) + \frac{\pi}{2}\left(r_{pf} + r_p\right)^2\right] \qquad (43)$$

or

$$A_c\,(\text{splatter/piece}) = \frac{4w\left(r_{pf} + r_p\right)}{r_{max}^2}\sum_{i=1}^{n}\left(r_{max} - r_i\right)\left[\left(Q_i\right) + \frac{\pi}{4}\left(r_{pf} + r_p\right)\right] \qquad (44)$$

where values of r_i are determined from Eq. (35), w is the interval width, r_{max} is the maximum splatter range for pieces projected from the impacting fragment, r_{pf} is the radius of the projected fragment, and r_p is the radius of a person. The quantity Q_i depends on the relative magnitudes of d_i, r_p, and r_i. Evaluation of Q_i can be clarified by referring to Fig. 13. For these four all-inclusive cases where the projected fragment rises above height h_p, values of Q_i are as follows:

Case 1: $d_i \geq r_p$. $\quad Q_i = 2d_i - r_p$

Case 2: $d_i < r_p$, and $r_i - d_i \geq r_p$. $\quad Q_i = d_i$

Case 3: $d_i < r_p$, $r_i - d_i < r_p$, and $r_i \geq r_p$. $\quad Q_i = r_i - r_p$

Case 4: $d_i < r_p$, $r_i - d_i < r_p$, and $r_i < r_p$. $\quad Q_i = 0$

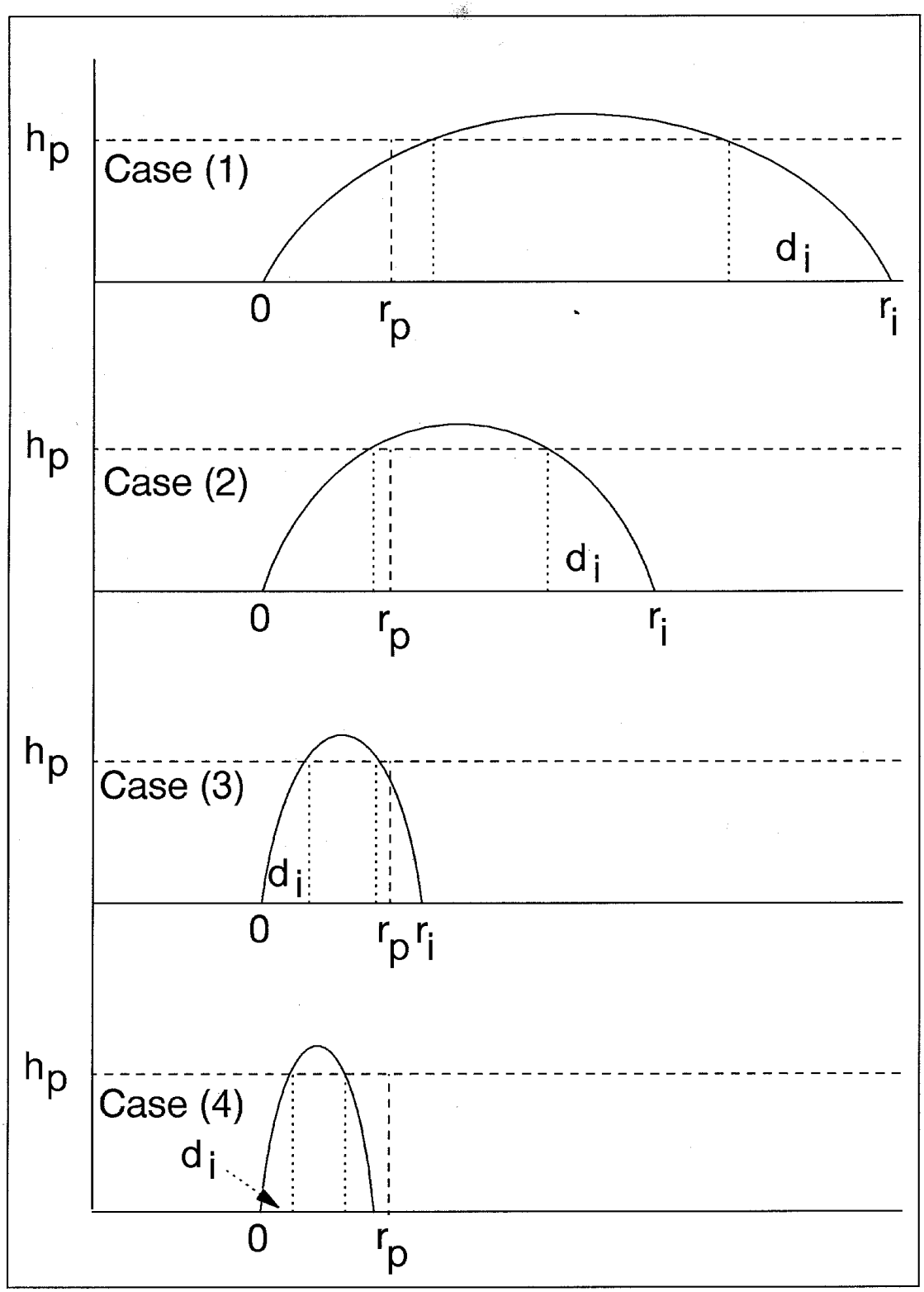

Figure 13. Fragment Trajectory Geometry

The last bracketed term in Eq. (43) is the effective casualty area for a single projected piece, given that the piece impacts in the i^{th} range interval. If there are N projected pieces, the conditional casualty area for the i^{th} interval can be obtained simply by multiplying the single-piece area by N, with the proviso that the product does not exceed some maximum value. This value, termed $A_i(max)$, is the maximum possible area that the projected fragments can endanger while simultaneously moving beyond the horizontal distance r_p and above height h_p. For Case (1), $A_i(max)$ is the sum of the shaded areas shown in the plan view of Fig. 14. The sum is easily determined to be

$$\textit{Case}\ (1): \quad A_i(max) = \pi\left(2\,r_f d_i + 2\,r_i d_i - 2 r_f r_p - r_p^2\right) \tag{45}$$

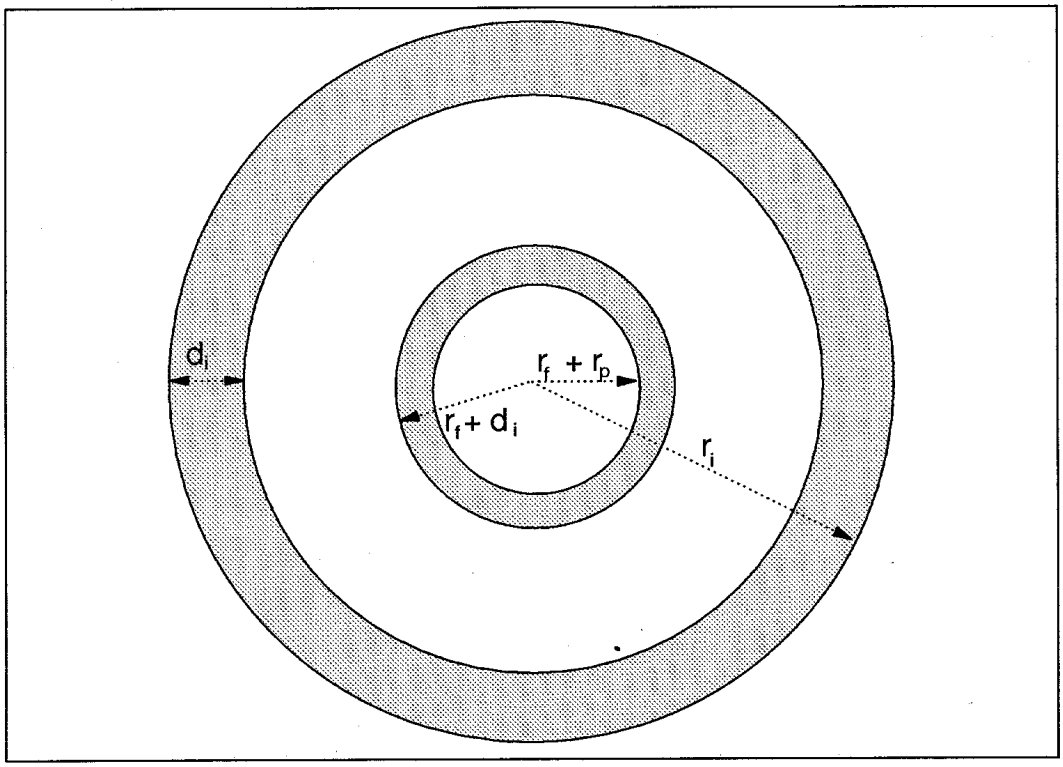

Figure 14. Limits on Casualty Area for Splatter

Similar diagrams can be drawn and maximum areas computed for the other cases depicted in Fig. 13, with the following results:

$$\begin{aligned} &\textit{Case}\ (2): \quad A_i(max) = \pi d_i\left(2\,r_i - d_i\right) \\ &\textit{Case}\ (3): \quad A_i(max) = \pi r_p\left(2\,r_i - r_p\right) \\ &\textit{Case}\ (4): \quad A_i(max) = 0 \end{aligned} \tag{46}$$

If for the i^{th} interval, $A_i(max)$ is less than N times the casualty area for a single projected piece, $A_i(max)$ is substituted instead for the last bracketed term in Eq. (43).

Equation (44) or Eq. (43) gives the effective casualty area for a single projected piece. The issue of the number of pieces projected from an impacting component is discussed later in Section 8.7. If N pieces are projected, each term in Eq. (43) must be multiplied by N or replaced by $A_i(max)$. The total casualty area due to splatter for the component may then be represented by the equation

$$A_c(\text{splatter/component}) = \sum_{i=1}^{n} \left\{ \textit{Maximum of} \left[N A_c(\text{splatter/piece})_i , A_i(max) \right] \right\} \quad (47)$$

As a modification to the foregoing, there is some minimum velocity that a projected piece must acquire before it is considered hazardous. According to data presented by Ahlers[9], the threshold for serious injury for one to two-pound pieces is about 15 feet/second. Lighter pieces require greater velocities to do serious injury, while pieces heavier than about two pounds need slightly less than 10 feet/second. Although somewhat arbitrary, for use in computing effective splatter areas a threshold velocity of 10 feet/second (corresponding to a maximum impact distance of 3.1 feet) has been selected. This velocity is acquired by the piece in falling from a height of 1.6 feet. Thus, if a piece is projected at a velocity so low that it cannot impact more than 3.1 feet from the periphery of the impacting fragment, the effective splatter area is assumed to be zero for the projected piece. To put it another way, if r_{max} for an impacting piece is less than 3.1 feet, the splatter area for that piece is zero.

8.6 Maximum Splatter Range

Before the effective splatter area (i.e., the casualty area due to splatter) can be evaluated for an impacting component, the maximum splatter range r_{max} and the number of splatter pieces must be established for the component. To a large extent, the maximum hazardous splatter range for an impacting inert component is a matter of engineering judgment. It seems reasonable to assume that it is some rather complicated function of kinetic energy per unit area (rather than kinetic energy), although many imponderables exist, e.g., shape, mass, orientation, and composition of the impacting component, impact velocity, properties of the impacted terrain, energy lost in cratering and in crumpling and tearing apart the impacting component. In impact experiments with steel spheres[10] where both the impacting and impacted materials were fairly reproducible, the results varied a great deal. Depth of penetration, for example, was not predictable to better than a factor of two even when projectile parameters and impacted materials were well known. The following is quoted from Section III of Ref. [10], which discusses the non-predictability of the effects of impact:

> In making operational plans based on damage predictions, it must be borne in mind that the confidence level of prediction is inherently low. Even in well-controlled laboratory determination of damage, wide scatter is commonly obtained in the data for supposedly identical specimens tested under repeatable conditions. · · · It is because of the inherent nonreproducibility of practical impact situations that the approximate and quick prediction methods presented here are valuable. More 'accurate' calculations will usually provide only the illusion of accuracy.

In view of this, it seems apparent that only "ball-park" approximations can be developed for highly diverse and deformable components that impact at various velocities in unpredictable attitudes on uncertain terrain. Since no pertinent experimental data are available, these difficulties must be tossed aside if progress is to be made.

Kinetic energy (KE) is computed from a component's weight W and impact speed v using the equation

$$KE = \frac{1}{2} m v^2 = \frac{1}{2} \frac{W}{g} v^2 \qquad (48)$$

where g is the mass to weight conversion factor. For use with program DAMP, the component's impact speed is computed by numerically integrating the equations of motion to impact, although the speed may also be approximated from the terminal-velocity equation [Eq. (12)]. Although a relationship between kinetic energy and splatter range could have been assumed, RTI's visceral feeling is that KE per unit area is a better parameter for correlation. Some confidence is gained for the assumption by noting penetration equations presented in Section 3.1 of Ref. [10], although depth of penetration and maximum splatter range are not necessarily functions of the same parameters. Using experimental test data, Kornhouser found that depth of penetration Y could be represented by the expression $Y = CWv^2/D^2$, where C is a proportionality constant and W, v, and D are the impacting projectile's weight, striking speed, and diameter. It can be noted that the numerator of the expression for Y is proportional to kinetic energy and the denominator is proportional to area. As a numerical example further suggesting that KE/A is a reasonable correlation parameter, consider a 1000-pound piece impacting at 200 ft/sec that has the same KE as a 16,000-pound piece that floats down on a parachute at 50 ft/sec. Other things being equal, common sense suggests that breakup and splattering from the 1000-pound piece should be more extensive. In all likelihood, the cross-sectional area of the 16,000-pound piece would be considerably greater than the corresponding area of the 1000-pound piece, resulting in a smaller KE/A for the heavier piece.

According to Chemical Propulsion and Information Agency (CPIA) Publication 394, page 2-47, Henny and Carlson[11] found that the maximum range of crater ejecta from

surface explosions scaled as the 0.4 power of the explosive weight. For rock and soil media, the maximum distances in feet were represented as follows:

$$r_{max}(\text{rock}) = 70\, W_{TNT}^{0.4} \tag{49}$$

$$r_{max}(\text{soil}) = 30\, W_{TNT}^{0.4} \tag{50}$$

where W_{TNT} is the TNT weight in pounds.

According to the same CPIA publication, page 2-18, Ahlers[12] developed a similar relationship for maximum debris range based on data from 206 accidental and planned explosions. Applying regression-analysis techniques, he arrived at the following relationship for maximum distance without regard for type of surface, where W_{TNT} is in pounds of TNT and r_{max} is in feet.

$$r_{max}(\text{explosion}) = 77\, W_{TNT}^{0.322} \tag{51}$$

Equations (51) and (49) give the same answers for W = 3.4 pounds. For heavier weights, Eq. (49) gives larger values, and for lighter weights, somewhat smaller values. Since the composition or nature of the impacted surface is always uncertain and since most splatter fragments are expected to come from breakup of the impacting body rather than the impacted surface, for hard surfaces maximum splatter ranges for inert debris will be based on Eq. (51) rather than Eq. (49). For soft surfaces, Eq. (50) is used. As mentioned earlier, the maximum splatter distance applied in calculating the effective splatter area – and used with the density function in Fig. 9 – is the maximum hazardous distance, not the maximum possible distance. Since Eq. (51) gives the mean value of the maximum projection distance, approximately half the 206 accidental explosions projected debris to greater ranges. In part, these greater distances are due to roll or bounce that occurred after initial impact. Since a projected piece is not as hazardous, or hazardous at all, as it tumbles or rolls along the ground to a stop, Eq. (51) is assumed to represent the maximum hazardous distance for debris projected from either an inert impact or an explosion.

As stated previously, the maximum splatter distance r_{max}(splatter) is assumed to be a function of kinetic energy per unit area. It is further postulated that r_{max}(splatter) is equal to r_{max}(explosion), where r_{max}(splatter) is calculated from Eq. (51) after impact kinetic energy has been scaled and then converted into equivalent pounds of TNT. If W_{TNT} is proportional to KE/A, then

$$W_{TNT}(\text{lb}) \propto \frac{w v^2}{2gA} \frac{\text{ft-lb}}{\text{ft}^2} \times \frac{1\ \text{lb TNT}}{1.54 \times 10^6\ \text{ft-lb}} \tag{52}$$

where kinetic energy is converted into pounds of TNT using the standard energy release for TNT of 10^9 calories per ton or 1.54 ft-lb/pound of TNT. This proportionality can be written in equation form as

$$W_{TNT}\,(\text{lb}) = \frac{k \times KE/A}{1.54 \times 10^6} \tag{53}$$

where, without loss of generality, the area A will be chosen in square feet, so the proportionality constant k, which has yet to be established, will also be in square feet. Ideally k – which may not be a constant at all but rather some function of w, v, and A – should be evaluated from experimental data.

Equation (51) and an energy transfer similar to that represented by Eq. (53) appeared in an earlier RTI working paper[13]. No claim was made then or has ever been made by RTI that the two types of energy will produce the same splatter effects. Rather, since explosions are considered to be more effective in projecting fragments and crater ejecta than equivalent-energy impacts, the use of Eqs. (53) and (51) with a suitable value of k should provide a conservative upper limit for the maximum hazardous distance to which debris can be splattered by inert impacts.

Since no experimental data were available for evaluating k in Eq. (53), a subjective procedure was used. To this end, values of r_{max} were calculated from Eqs. (53) and (51) for several impacting bodies using arbitrarily assigned values of k. Body characteristics are given in Table 10 and results in Table 11. From an inspection of these results, a value of k must be chosen.

Table 10. Component Characteristics

Item No.	Atlas IIAS Component	Weight (lbs)	w/C_dA (lb/ft^2)	Area (ft^2)	Terminal Velocity (ft/sec)	KE/A ($ft\text{-}lb/ft^2$)
1	Turbo-pump assembly	1056	190	7.94	408	3.44×10^5
2	Expended Castor IVA	1550	98.8	8.77	294	2.37×10^5
3	Centaur engine assembly	442	51.2	13.0	212	2.37×10^4
4	Interstage adapter	1206	10.3	72.0	94.9	2.34×10^3
5	Jettison rail	33	6.6	4.78	76.0	6.20×10^2

Table 11. Maximum Splatter Range (r_{max})

	Max Splatter Range (ft) for Items in Table 7				
k (ft^2)	1	2	3	4	5
1.0	47.5	42.1	20.1	9.5	6.2
0.8	44.2	39.2	18.7	8.9	5.8
0.6	40.3	35.8	17.0	8.1	5.3
0.4	35.4	31.4	15.0	7.1	4.6
0.2	28.3	25.1	12.0	5.7	3.7
0.1	22.6	20.1	9.6	4.5	3.0

Although perhaps trivial, Eq. (53) can be applied to TNT if the kinetic energy released by an explosion is assumed to occur over an area of one square foot and the constant k is set equal to one. Since intuition suggests that TNT should be more effective in propelling pieces than an equivalent-energy impact, it seems logical to use a value of k less than one in calculating maximum splatter range. Due to the lack of experimental data, subjective considerations cannot be avoided in choosing a value. For example, just how close would a person located on a hard surface willingly stand to a 1056-pound turbopump assembly (Item No. 1) that impacts at 408 ft/sec? Practical experience fails because impacts witnessed in life are, for the most part, at much lower velocities. Although intuition is not necessarily a good guide, RTI has answered the turbopump-distance question raised above by choosing k = 0.6 ft^2. Since there seemed to be no good reason for doing otherwise, **a value of k = 0.6 was chosen** for all other impacting inert components as well.

For pieces resulting from vehicle breakup, a kinetic-energy threshold has been implicitly established by assuming that **the splatter area is zero unless r_{max}(splatter) exceeds 3.1 feet.** Below this threshold, hazardous splattering will not occur. Instead, the impacting piece may slide or skid, or may deform and bounce without breaking apart. Applying Eq. (51) with r_{max}(explosion) = 3.1 feet and converting pounds of TNT into ft-lbs of energy using Eq. (53) with k = 0.6, the threshold for splatter becomes approximately 120 ft-lbs/ft^2. This kinetic energy is achieved by a one-square-foot body having a ballistic coefficient and weight per unit area of 3 lbs/ft^2 and a terminal velocity of 51 ft/sec.

8.7 Number and Weight of Splatter Fragments

Having established procedures for estimating the effective splatter area if N pieces are projected from an impacting component or fragment, a numerical value must be derived

(or assumed) for N before the total effective splatter area can be computed for the impacting fragment. The only pieces of interest are those projected beyond the periphery of the impacting component in accordance with the density function, f(r), shown in Fig. 9. As pointed out previously, no experimental or accident data for impacting inert pieces could be found to serve as a guide.

In general, most splatter pieces are expected to originate from the impacting body rather than the impacted surface, since cratering may not occur at all except for fragments with large ballistic coefficients. If this is the case, the number of splatter pieces should be related in some way to the mass of the impacting body. Other imponderables add to the uncertainty of estimating the number of splatter fragments produced. For example, a module consisting of many individual components will likely produce more splatter fragments than a more homogenous body with the same weight and KE/A, although even this depends on the frangibility of the impacting body.

To make progress, some assumptions must be made about the average number of projected pieces produced by an inert impact, even though the assumptions are conjectural in nature. Although no empirical data could be found for inert impacts, limited data from five accidental space-vehicle explosions were discovered in CPIA Publication 394[14]. For these relatively large explosions where the TNT equivalency was estimated to be 1000 pounds or more, the number of recovered pieces varied from 40 to 949. For the two smallest explosions, both with estimated yields of 1000 pounds, 44 and 60 projected pieces were recovered. It seems likely that other pieces were not found or were considered too small to be of interest even though small high-speed projectiles may be hazardous to people in the open. Fragment data from the five accidents are given in Table 12.

Table 12. Fragment Data from Vehicle Accidents

Test Vehicle (accident date)	Total Fragment Weight (lb)	TNT Yield (lb)	No. of Pieces Recovered
Atlas Centaur (3-2-65)	9085	1930	40
S-IVB-ASTV (1-24-64)	1882	1000	44
S-IV-EAFB (7-14-65)	3125	3200	412
S-IVB-503 (1-20-67)	1426	2300	949
PYRO-275 (3-22-67)	1628	1000	60

For the five vehicle accidents, the CPIA Publication (Fig. 2-35) provides graphs of total fragment weight in percent versus fragment range from the explosion in feet. Since the plot for PYRO-275 was incomplete, it was discarded. In other cases, graphs were either

redrawn to pass more closely to plotted data points or extrapolated to zero percent. Percentages read from the remaining four curves, as modified, are given in Table 13.

Table 13. Percent of Total Weight of Fragments Within Indicated Range

Range (ft)	Atlas Centaur	S-IVB-ASTV	S-IV-EAFB	S-IVB-503
1000	-	-	101	98
900	-	97.5	100	94
800	-	97.5	97	90
700	-	97	91	88
600	-	96.5	82.5	86
500	101	93	71	80
400	99	80	55	66
300	94	49	49	50
200	82	18	17	31
100	41	4	0	11
50	0	0	-	0

The data in Tables 12 and 13 will now be used to estimate the total kinetic energy imparted to vehicle fragments by their respective explosions. By differencing percentages in Table 13 and multiplying by the total fragment weight given in Table 12, the weight of fragments impacting in each range interval can be found. If a ballistic coefficient and initial path angle are assumed, the projection velocity needed to produce impact at the midpoint of each range interval can be calculated. With fragment weight and velocity determined for each range interval, the KE can be calculated and then summed for all intervals. This energy can be converted into equivalent pounds of TNT, then divided by the yield in Table 12 to provide an estimate of the percent of explosive energy that is effective in propelling fragments away from the explosion.

Since the effective ballistic coefficient (β) of the fragments and initial projection angles (γ) were unknown, computations were made for several values of each parameter. Results are given in Tables 14 and 15 for the S-IVB-EAFB accident at Edwards Air Force Base, where the foot-pounds of kinetic energy shown in Table 14 have been converted into equivalent pounds of TNT in Table 15. For smaller values of β, the velocity needed to reach the midrange of the longer range intervals was several thousand feet per second. According to CPIA Publication 394 (Vol. 1, September 1984), Baker[15] established from Project Pyro data and explosions of other liquid-propellant motors that the mean initial fragment velocity from liquid-propellant explosions could be represented by the equation

$$v = 74\, W^{0.4296} \tag{54}$$

where W is the explosive yield in pounds of TNT. If, for any β, the velocity required to reach the midrange of the interval exceeded the velocity given by Baker's equation, the value of β was doubled and the velocity recalculated. The doubling was continued until a suitable velocity was obtained to use in the kinetic-energy calculations.

Table 14. Estimates of Kinetic Energy (ft-lb x 10^7) Imparted to Fragments For the S-IVB-EAFB Accident

	Initial Projection Angle (γ)				
β (lb/ft^2)	15°	30°	45°	60°	75°
5	5.2	2.1	4.9	3.9	4.9
10	1.3	1.1	1.7	3.4	4.4
20	0.28	0.18	0.19	0.38	2.8
40	0.17	0.10	0.096	0.13	0.47
80	0.14	0.086	0.076	0.093	0.20

Table 15. Estimates of Kinetic Energy (lb. of TNT) Imparted to Fragments For the S-IVB-EAFB Accident

	Initial Projection Angle (γ)					
β (lb/ft^2)	15°	30°	45°	60°	75°	Mean
5	34	14	32	25	32	27.4
10	8.3	6.8	11	22	29	15.4
20	1.8	1.2	1.2	2.5	18	4.94
40	1.1	0.68	0.63	0.84	3.0	1.25
80	0.94	0.56	0.49	0.60	1.3	0.78
					Mean	9.95

Since ballistic coefficients and initial path angles of fragments projected from an explosion vary considerably, the results in Tables 14 and 15 based on quasi-constant ballistic coefficients and path angles are, at best, rough estimates. Nevertheless, some KE estimate must be established, so RTI has assumed that the mean of the 25 entries in Table 15 (or Table 14) produces the best estimate of the total KE acquired by vehicle fragments. The percent of explosive energy imparted to the projected pieces in the form of kinetic energy for the S-IVB-EAFB accident is found by dividing the mean of 9.95 pounds of TNT by the TNT yield from Table 12. The results from this and three other vehicle accidents (not including PYRO-275) are given in Table 16. For the four accidents, the mean percentage of explosive energy converted into kinetic energy was computed to be 0.19%.

Table 16. Percent of Explosive Energy Converted into Fragment Kinetic Energy

Accident Vehicle/Stage	Energy Converted to KE (%)
Atlas Centaur	0.14
S-IVB-ASTV	0.18
S-IV-EAFB	0.31
S-IVB-503	0.13
Mean	0.19

The following assumptions will now be made:

(1) If the impacting body weighs less than 0.25 pounds, the splatter effect is negligible (zero).

(2) For hard surfaces, the percentage of the kinetic energy of an impacting inert body that is transferred to the splatter fragments is 0.095%. This is half the estimated mean percentage of explosive energy that was converted into kinetic energy in projecting fragments from the four explosions listed in Table 16. For soft surfaces, the percentage of energy transferred to the splatter fragments is one-fourth that for hard surfaces.

(3) The weight of the heaviest possible projected piece is equal to the weight of the impacting body. The weight of the smallest, hazardous, projected piece is 0.25 pound.

(4) The number of projected pieces is normally distributed with respect to the natural logarithm of piece weight, with the logarithms of the maximum and minimum weights, as defined in assumption (3), considered to be ± 3-sigma values. The weight of the mean projected piece thus becomes

$$w_{mean} = \exp\left(\frac{\log_e w_{max} + \log_e w_{min}}{2}\right) \tag{55}$$

The average KE required to project the mean piece to ranges between zero and r_{max}(splatter) can now be calculated for any impacting body. Referring to the density function [f(r)] in Fig. 9, the distance r_{max} is divided into n intervals. For each interval, the kinetic energy needed for the mean splatter piece to reach the midpoint of the interval is calculated for initial projection angles of 15°, 30°, 45°, 60° and 75°. The mean of the five KE values is computed and designated as KE_i(mean). Because splatter ranges

and the velocities needed for splatter fragments to reach these ranges are small, vacuum calculations can be made in evaluating kinetic energies without significant error. The weighted KE for each interval is calculated as the product of the mean KE needed for the mean piece to reach the midpoint of the interval and the probability that the piece impacts in the interval. The range r_i to the midpoint of the i^{th} interval is given by Eq. (35), and the probability of impacting in the interval by Eq. (36), where the interval width $w = r_{max}/n$. The total average KE imparted to the mean projected fragment can be written in equation form as follows:

$$\text{KE(mean projected fragment)} = \sum_{i=1}^{n} \left[\dot{KE}_i(\text{mean})\right]\left[\text{Prob}(r_i)\right] \tag{56}$$

where $KE_i(\text{mean})$ is the mean kinetic energy needed by the mean projected fragment to reach range r_i.

The total number of projected pieces can now be estimated by dividing the percentage of KE of the impacting body that is transferred to projected fragments by the KE of the mean projected fragment determined from Eq. (56). In equation form,

$$N = \frac{(F)\,(\text{KE of impacting body})}{\text{KE(mean projected fragment)}} \tag{57}$$

where N is the number of projected fragments and F* is the fraction of the kinetic energy of the impacting body that is transferred to the projected pieces. Although Eq. (57) does not generally produce an integral number of pieces, the use of fractional pieces in the casualty-expectancy calculations causes no difficulty.

Like many assumptions in this report, assuming that F_h for hard surfaces is four times as large as F_s for soft surfaces cannot be fully justified. Intuition certainly suggests that, for a soft-surface impact, considerably more impact energy will be consumed in displacing impacted material laterally and throwing it from the resulting crater. If the coefficient of restitution for a hard-surface impact is about twice that for soft surfaces, which does not seem unreasonable, a piece rebounding from a hard surface will be four times as energetic as the same piece rebounding from a soft surface. Intuition further suggests that the number of splatter fragments produced by a soft-surface impact should be about the same as, or somewhat less than, the number resulting from a hard-surface impact. Using a value of $F_h = 4F_s$ in Eq. (57) seems consistent with this notion.

---

* The subscripts h and s are used to designate kinetic-energy fractions for hard and soft surfaces, respectively.

8.8 Frangibility Factor

As mentioned earlier, the number of splatter fragments produced by an impacting body depends on its composition since a module, instrumentation section, or fragile payload consisting of many components would presumably produce more splatter fragments than, for example, a rigid helium sphere. This presumption is at least partially confirmed by a report[16] that shows pictures of helium spheres and other rigid components that have survived both orbital reentry and impact essentially intact.

To account for compositional differences in impacting bodies, Eq. (57) has been modified as shown in Eq. (58) by the inclusion of a frangibility factor f that varies between zero and one. A value of f = 1 is assigned to a body that is considered highly frangible, while f = 0 is used for a body that is not expected to break up or project debris after impact. Bodies of intermediate frangibility are, of course, assigned intermediate values.

$$N = \frac{(f)\,(F)\,(\text{KE of impacting body})}{\text{KE(mean projected fragment)}} \tag{58}$$

Although inclusion of a frangibility factor in the equation for N seems logically sound, some procedural problems arise in application:

a. The composition of pieces resulting from vehicle breakup may not be known sufficiently well to make realistic choices for f.

b. Another consideration – in addition to ballistic coefficient, breakup velocity, weight, and area – is introduced in classifying breakup debris. Thus it may be necessary to split debris that is now placed in a single class into two or more classes.

In view of practical problems, a value of f = 0.5 is used to develop casualty areas for splatter when knowledge of debris composition or the results of impact are too uncertain to permit a logical choice for f.

8.9 Size of Splatter Fragment

As seen from Eq. (44), the radius of the projected fragment r_{pf} is needed to calculate effective casualty area. Since some value or relation must be established, it seems reasonable to assume that r_{pf} is proportional to fragment weight, or rather to the mean weight of all fragments projected from the impacting body. Remembering that the weight of the largest projected piece is assumed to be the weight of the impacting body and the weight of the smallest piece is 0.25 pounds, a linear relationship was established between the radius of the mean piece and the logarithm (base 10) of its weight. The smallest piece was assumed to have a radius of one inch, while a piece weighing 10 pounds was given a radius of 12 inches. In equation form, the relationship becomes:

$$r_{pf} = 5.13 + 6.87 \log_{10} w_{mean} \quad (59)$$

Using this equation produces the projected-fragment sizes shown in Table 17.

Table 17. Sample Projected Fragment Sizes

Mean Piece Weight (lb)	Projected Fragment Radius (inches)
0.25	1.00
1	5.13
3	8.41
10	12.0
30	15.3
100	18.9
300	22.1
1000	25.7

Using the procedures outlined in this section and the Atlas IIAS components listed in Table 10, the maximum splatter range, number of splatter fragments, and mean splatter-fragment weight and radius are shown in Table 18. Although the number of splatter fragments can be made integral, fractional numbers can be used in the risk calculations.

Table 18. Sample Splatter Parameters for Hard-Surface Impacts

Atlas IIAS Components	Max Splatter Range (ft)	Number of Splatter Fragments	Mean Splatter Frag Weight (lb)	Mean Splatter Fragment Radius (in)
Turbo-pump assembly	40.3	16.2	16.2	13.4
Expended Castor IVA	35.8	11.5	19.7	14.0
Centaur engine assembly	17.0	6.7	10.5	12.1
Interstage adapter	8.1	4.7	17.4	13.6
Jettison rail	5.3	0.8	2.9	8.3

8.10 Attempt to Obtain Experimental Data

The results obtained using Eqs. (53) and (51) to establish maximum splatter ranges for impacting inert bodies are admittedly subject to considerable uncertainty. A similar statement can be made about the use of Eqs. (58) and (55) to estimate numbers and mean weights of splatter pieces. In an effort to obtain experimental data on which to base assumptions and thus increase confidence in the results, RTI wrote to the National Transportation Safety Board requesting information on debris scatter from high-speed, near-vertical, non-explosive, aircraft impacts. In response[17], NTSB provided information on seven accidents where the aircraft impact angles varied between 45° and 85°. Three of the seven had estimated impact angles between 80° and 85° with impact speeds from 363 ft/sec to 507 ft/sec. The numbers of pieces with recorded locations varied from 39 to 114 with no weights given. A study of the debris diagrams from these latter three accidents showed that aircraft parts and pieces were scattered several hundred feet from the main-body impact craters. Additional information about the crashes, such as the following, are needed if the data are to be useful in estimating splatter parameters:

a. Aircraft heading just before and at impact
b. Aircraft breakup or breakaway of pieces before impact
c. Extent to which scatter of pieces was due to effects of winds after impact, or to pieces tumbling down inclines.
d. Extent to which pieces were scattered by a deflagration at impact
e. Wind speed and direction after impact before piece locations were recorded
f. Characteristics of dispersed pieces
g. Weights and total numbers of pieces

Since the needed information was not provided and seems unlikely to be forthcoming, the data provided by the NTSB has not been used in formulating splatter-model parameters. If information on these or other accidents or incidents should become available in the future, procedures for modeling splatter parameters should be revisited.

9. Composite Casualty Area

Before the total effective casualty area for an inert debris class can be calculated, a composite casualty area must be determined for the mean piece in the class. The cross-sectional area of the mean piece augmented by wind and impact-angle effects is accounted for by using Eq. (4). To this area must be added the casualty area due to one of the following:

(1) Slide or skid: Eq. (6)

(2) Bounce:
For the i^{th} rebound angle:
Bounce height $\leq h_p$: Eq. (18)
Long bounce with bounce height $> h_p$: Eq. (22)
Short bounce with bounce height $> h_p$: Eq. (26)
Weighted sum for all rebound angles: Eq. (32)

(3) Splatter: Eqs. (44) and (47)

As defined in this report, the three augmenting effects are mutually exclusive, since an impacting piece that bounces intact cannot simultaneously break up or slide along the ground, and since a piece that slides or bounces remains essentially intact while one that splatters is assumed to break apart.

In earlier RTI studies[18],[19], the inert pieces produced by destruct breakup of Atlas IIAS and Delta-GEM vehicles have been separated into debris classes, according to piece characteristics. To illustrate the results of procedures developed in this report, casualty areas have been computed for the mean piece in each debris class. Results are presented in the appendices.

Appendix A. Effective Casualty Areas for Atlas IIAS Debris

Atlas IIAS debris characteristics[18] are summarized in Table A1. To prepare effective casualty areas for standard risk calculations in DAMP, impact velocities are computed as functions of failure time. For expediency, the effective casualty areas shown in this appendix are computed for terminal-velocity conditions instead.

Intermediate results associated with splatter calculations are given in Table A2. Although considerable uncertainty is involved, a frangibility factor has been assigned to each debris class. Numbers of splatter fragments and maximum splatter range are provided for impacts on both hard and soft surfaces.

The path angles of the velocity vectors at impact are computed using the terminal velocity as the vertical component and the mean annual wind speed for Cape Canaveral (11.5 feet per second) as the horizontal component. The effective casualty areas for the four effects discussed in this report are given in columns 2 through 5 of Table A3 for hard-surface impacts, and Table A4 for soft-surface impacts. These are:

(1) A_{basic}: the **basic** effective casualty area, computed from the cross-sectional area of the piece, the assumed dimensions of a person in the open, and the path angle of the velocity vector at impact, discussed in Section 5,

(2) A_{slide}: additional casualty area from slide or skid, discussed in Section 6,

(3) A_{bounce}: additional casualty area from bounce or ricochet, discussed in Section 7,

(4) A_{splat}: additional casualty area from splattering and cratering, discussed in Section 8. Splatter parameters are given in Table A2.

The composite casualty area A_{eff} considering all four effects is given in column 6 of Table A3 for hard surfaces, and Table A4 for soft surfaces. It is obtained by adding the largest of the areas due to slide, bounce, and splatter to the basic area, as discussed in Section 9.

The last column of Tables A3 and A4 shows the ratio of the composite effective casualty area to the basic casualty area, i.e., the casualty area due to a piece falling diagonally.

Table A1. Atlas IIAS Debris Characteristics

Class	Description	Weight (lb)	Cross-sect. Area (ft^2)	Subsonic β (lb/ft^2)	Terminal Vel. (ft/sec)
A1	Tank frags	2.99	3.53	0.98	29.3
A2	Tank frags	14.75	16.04	1.05	30.3
A3	Tank frags	6.16	5.38	1.24	32.9
A4	Tank frags	18.22	13.85	1.54	36.7
A5	Tank frags	4.31	2.91	1.72	38.8
A6	Prestart solenoid	0.15	0.06	2.10	42.9
A7	Miscel. frags	46.57	20.08	2.61	47.8
A8	Miscel. frags	4.95	0.68	4.66	63.9
A9	Miscel. frags	1.80	0.37	4.89	65.4
A10	Miscel. frags	31.70	6.24	5.06	66.5
A11	LO2 inlet elbow	11.00	1.42	8.60	86.8
A12	Large payload fairing	1908.	61.33	9.63	91.8
A13	Major frags	5.00	0.43	10.16	94.3
A14	Major frags	216.	16.35	12.30	103.8
A15	Major frags	13.51	1.15	16.89	121.6
A16	Miscel. frags	8.49	0.34	25.06	148.1
A17	Miscel. frags	1.43	0.05	25.34	148.9
A18	Miscel. frags	39.75	1.88	27.55	155.3
A19	Major frags	1236.8	33.64	36.04	177.6
A20	Major frags	65.47	2.83	43.06	194.1
A21	Major frags	315.67	9.03	50.33	209.9
A22	Miscel. frags	4.10	0.04	100.00	295.9
A23	Miscel. frags	43.26	0.43	100.00	295.9
A24	Booster turbo pump	1056.	7.94	190.00	407.8
P1	Spacecraft frags	25.20	9.25	1.05	30.3
P2	Spacecraft frags	123.27	12.10	4.35	61.7
P3	Payload module	1115.8	29.90	14.60	113.0
P4	Spacecraft frags	85.71	2.80	14.74	113.6
P5	Bus module	5372.8	28.60	187.9	405.5
C1	Castor frags	5.36	2.74	2.09	42.8
C2	Castor frags	9.17	2.19	4.69	64.1
C3	Nozzle closure	40.00	5.58	7.20	79.4
C4	Castor frags	4.22	0.24	27.50	155.1
C5	ADJ thruster arm	65.00	1.53	70.80	248.9
C6 *	Castor prop. frags	18.00	0.30	133.	341.2
C7 *	Castor prop. frags	35.00	0.47	165.	380.0
C8 *	GL Castor (dest.)	14387.	107.5	555.	697.0
C9 *	AL Castor (dest.)	21936.	107.5	847.	861.0
C10 *	GL Castor (ISDS)	13711.	107.5	529.	680.5
C11 *	AL Castor (ISDS)	21713.	107.5	838.	856.4

* Weights for these classes taken at impact following failure at 20 seconds

Table A2. Atlas IIAS Splatter Parameters

Class	KE/A (ft-lb/ft^2)	Frangible factor	Mean wt. (lb)	Num. Splat. Frags		R_{max} (ft)	
				Hard	Soft	Hard	Soft
A1	13.0	0.1	0.9	0.0	0.0	1.5	0.2
A2	15.0	0.2	1.9	0.1	0.1	1.6	0.2
A3	21.7	0.1	1.2	0.0	0.0	1.8	0.3
A4	30.3	0.2	2.1	0.1	0.1	2.0	0.3
A5	37.7	0.1	1.0	0.0	0.0	2.1	0.3
A6	76.6	0.1	0.0	0.0	0.0	2.7	0.5
A7	87.1	0.8	3.4	0.6	0.8	2.8	0.5
A8	476.4	0.5	1.1	0.1	0.2	4.8	1.0
A9	333.6	0.5	0.7	0.1	0.1	4.3	0.8
A10	360.1	0.5	2.8	0.4	0.4	4.4	0.9
A11	922.1	0.2	1.7	0.1	0.1	6.0	1.3
A12	4,139.1	0.4	21.8	1.9	2.0	9.7	2.3
A13	1,630.9	0.5	1.1	0.2	0.2	7.2	1.6
A14	2,237.4	0.5	7.4	1.2	1.4	8.0	1.8
A15	2,723.1	0.4	1.8	0.3	0.3	8.5	1.9
A16	8,563.1	0.5	1.5	0.3	0.3	12.3	3.1
A17	9,916.6	0.5	0.6	0.1	0.1	12.9	3.3
A18	7,966.8	0.2	3.2	0.3	0.3	12.0	3.0
A19	18,099.0	0.9	17.6	7.7	7.3	15.6	4.1
A20	13,597.5	0.4	4.0	1.0	1.0	14.2	3.7
A21	24,004.0	0.8	8.9	4.4	4.1	17.1	4.6
A22	139,633.1	0.5	1.0	0.4	0.3	30.2	9.4
A23	137,051.1	0.5	3.3	1.2	0.9	30.0	9.3
A24	343,994.1	0.7	16.2	11.3	8.5	40.3	13.4
P1	44.5	0.2	2.5	0.1	0.1	2.3	0.4
P2	623.7	0.6	5.6	0.6	0.7	5.3	1.1
P3	7,487.7	0.8	16.7	3.5	3.6	11.8	2.9
P4	6,200.2	0.8	4.6	1.1	1.1	11.1	2.7
P5	480,528.6	0.8	36.6	25.9	19.0	44.9	15.3
C1	59.6	0.2	1.2	0.0	0.1	2.5	0.4
C2	275.7	0.1	1.5	0.0	0.1	4.1	0.8
C3	716.8	0.6	3.2	0.5	0.6	5.5	1.1
C4	6,613.4	0.5	1.0	0.3	0.3	11.3	2.8
C5	41,000.6	0.3	4.0	0.9	0.8	20.3	5.7
C6 *	108,668.8	1.0	1.0	2.1	1.8	27.8	8.5
C7 *	167,286.3	1.0	1.0	3.2	2.6	32.0	10.1
C8 *	1,010,605.6	1.0	60.0	123.2	85.0	57.0	20.7
C9 *	2,351,357.1	1.0	74.0	176.9	114.3	74.9	29.0
C10 *	918,013.6	1.0	58.6	118.3	82.2	55.3	19.9
C11 *	2,302,726.9	1.0	73.7	175.3	113.4	74.4	28.7

* Data for these classes taken at 20 seconds

Table A3. Atlas IIAS Effective Casualty Areas for Hard-Surface Impacts

Class	A_{basic} (ft^2)	A_{slide} (ft^2)	A_{bounce} (ft^2)	A_{splat} (ft^2)	A_{eff} (ft^2)	Ratio A_{eff}/A_{basic}
A1	23.04	16.94	21.63	0	44.67	1.9
A2	48.22	26.80	36.23	0	84.44	1.8
A3	26.41	18.98	29.52	0	55.93	2.1
A4	41.84	25.48	47.85	0	89.69	2.1
A5	19.08	16.13	32.99	0	52.07	2.7
A6	7.73	9.36	20.78	0	28.51	3.7
A7	49.29	29.00	70.34	0	119.63	2.4
A8	9.91	12.05	31.39	0.55	41.30	4.2
A9	8.50	11.04	28.55	0.32	37.05	4.4
A10	23.23	19.81	55.39	1.73	78.63	3.4
A11	11.45	13.75	37.97	0.64	49.42	4.3
A12	100.38	44.54	151.33	24.83	251.70	2.5
A13	7.90	11.26	30.65	1.19	38.56	4.9
A14	38.19	0	84.13	12.00	132.32	3.2
A15	9.91	0	36.65	2.80	46.57	4.7
A16	6.79	0	28.47	3.95	35.26	5.2
A17	5.03	0	23.64	1.40	28.67	5.7
A18	11.46	0	38.74	4.23	50.20	4.4
A19	60.66	0	89.61	120.73	181.40	3.0
A20	13.32	0	33.72	17.35	47.05	3.5
A21	24.60	0	36.64	90.04	114.64	4.7
A22	4.41	0	0.03	8.49	12.89	2.9
A23	6.54	0	0.04	33.78	40.32	6.2
A24	21.95	0	0	426.61	448.56	20.4
P1	35.54	22.33	30.18	0	65.72	1.8
P2	34.20	24.35	68.58	3.86	102.78	3.0
P3	57.41	0	109.65	51.26	167.06	2.9
P4	14.24	0	45.74	13.89	59.97	4.2
P5	52.07	0	0	734.24	786.31	15.1
C1	17.99	15.90	35.33	0	53.32	3.0
C2	14.53	15.08	40.40	0.16	54.93	3.8
C3	21.15	19.18	54.74	3.33	75.89	3.6
C4	6.25	0	26.84	2.88	33.10	5.3
C5	10.00	0	8.74	20.58	30.57	3.1
C6 *	5.81	0	0	54.78	60.69	10.3
C7 *	6.45	0	0	94.51	101.05	15.4
C8 *	148.94	0	0	1046.18	1194.93	8.0
C9 *	148.59	0	0	1521.39	1669.88	11.2
C10 *	148.99	0	0	1001.15	1149.94	7.7
C11 *	148.60	0	0	1507.53	1656.03	11.2

* Data for these classes taken at 20 seconds

Table A4. Atlas IIAS Effective Casualty Areas for Soft-Surface Impacts

Class	A_{basic} (ft^2)	A_{slide} (ft^2)	A_{bounce} (ft^2)	A_{splat} (ft^2)	A_{eff} (ft^2)	Ratio A_{eff}/A_{basic}
A1	23.04	12.10	5.41	0	35.14	1.5
A2	48.22	19.14	9.06	0	67.36	1.4
A3	26.41	13.56	7.38	0	39.97	1.5
A4	41.84	18.20	11.96	0	60.04	1.4
A5	19.08	11.52	8.36	0	30.60	1.6
A6	7.73	6.68	5.81	0	14.42	1.9
A7	49.29	20.72	21.91	0	71.21	1.4
A8	9.91	8.60	13.64	0	23.55	2.4
A9	8.50	7.89	12.55	0	21.06	2.5
A10	23.23	14.15	22.57	0	45.80	2.0
A11	11.45	9.82	15.14	0	26.59	2.3
A12	100.38	31.82	47.65	0	148.03	1.5
A13	7.90	8.04	11.84	0	19.74	2.5
A14	38.19	0	26.08	0	64.27	1.7
A15	9.91	0	10.03	0	19.94	2.0
A16	6.79	0	4.45	0	11.24	1.7
A17	5.03	0	3.67	0.35	8.70	1.7
A18	11.46	0	4.62	0	16.08	1.4
A19	60.66	0	3.14	9.00	69.66	1.1
A20	13.32	0	0.10	4.02	17.34	1.3
A21	24.60	0	0	11.28	35.87	1.5
A22	4.41	0	0	2.56	6.97	1.6
A23	6.54	0	0	9.88	16.41	2.5
A24	21.95	0	0	94.36	116.31	5.3
P1	35.54	15.95	7.55	0	51.48	1.4
P2	34.20	17.40	27.39	0	61.59	1.8
P3	57.41	0	29.06	0	86.47	1.5
P4	14.24	0	13.73	0	27.96	2.0
P5	52.07	0	0	123.96	176.03	3.4
C1	17.99	11.36	9.83	0	29.35	1.6
C2	14.53	10.77	17.09	0	31.62	2.2
C3	21.15	13.70	21.72	0	42.87	2.0
C4	6.25	0	3.34	0	9.60	1.5
C5	10.00	0	0	5.26	15.26	1.5
C6 *	5.81	0	0	15.41	21.32	3.6
C7 *	6.45	0	0	27.32	33.87	5.2
C8 *	148.94	0	0	216.27	365.02	2.5
C9 *	148.59	0	0	377.35	525.84	3.5
C10 *	148.99	0	0	202.27	351.06	2.4
C11 *	148.60	0	0	372.31	520.81	3.5

* Data for these classes taken at 20 seconds

Appendix B. Effective Casualty Areas for Delta Debris

Delta-GEM debris characteristics[19],[20] are summarized in Table B1. To prepare effective casualty areas for standard risk calculations in DAMP, impact velocities are computed as functions of failure time. For expediency, the effective casualty areas shown in this appendix are computed for terminal velocity conditions instead.

Intermediate results associated with splatter calculations are given in Table B2. Although considerable uncertainty is involved, a frangibility factor has been assigned to each debris class. Numbers of splatter fragments and maximum splatter range are provided for impacts on both hard and soft surfaces.

The path angles of the velocity vectors at impact are computed using the terminal velocity as the vertical component and the mean annual wind speed for Cape Canaveral (11.5 feet per second) as the horizontal component. The effective casualty areas for the four effects discussed in this report are given in columns 2 through 5 of Table B3 for hard-surface impacts, and Table B4 for soft-surface impacts. These are:

(1) A_{basic}: the **basic** effective casualty area, computed from the cross-sectional area of the piece, the assumed dimensions of a person in the open, and the path angle of the velocity vector at impact, discussed in Section 5,

(2) A_{slide}: additional casualty area from slide or skid, discussed in Section 6,

(3) A_{bounce}: additional casualty area from bounce or ricochet, discussed in Section 7,

(4) A_{splat}: additional casualty area from splattering and cratering, discussed in Section 8. Splatter parameters are given in Table B2.

The composite casualty area A_{eff} considering all four effects are given in column 6 of Table B3 for hard surfaces, and Table B4 for soft surfaces. It is obtained by adding the largest of the areas due to slide, bounce, and splatter to the basic area, as discussed in Section 9.

The last column of Tables B3 and B4 shows the ratio of the composite effective casualty area to the basic casualty area, i.e., the casualty area due to a piece falling diagonally.

Table B1. Delta-GEM Debris Characteristics

Class	Description	Weight (lb)	Cross-sect. Area (ft^2)	Subsonic β (lb/ft^2)	Terminal Vel. (ft/sec)
D2	Miscel. Delta frags	2.28	3.20	0.88	27.8
D3	Miscel. Delta frags	9.20	4.83	2.47	46.5
D4	Propellant tank frags	104.	26.02	4.60	63.5
D5	Fairing, skirt, etc.	117.	3.57	8.41	85.8
D6	Miscel. Delta frags	3.41	0.28	9.05	89.0
D7	Nosecone fairing	448.	52.25	10.50	95.9
D8	Miscel. Delta frags	45.4	2.10	17.14	122.5
D9	Miscel. Delta frags	4.97	0.17	17.69	124.4
D10	Miscel. Delta frags	273.	8.53	18.78	128.2
D11	Miscel. Delta frags	16.0	0.17	30.66	163.8
D12	Small tanks, nozzle	56.0	2.58	35.08	175.2
D13	RS-27 Stage I engine	2242.	46.67	69.90	247.3
D14	Miscel. Delta frags	87.3	2.26	59.20	227.6
D15	Miscel. Delta frags	22.2	0.34	60.12	229.4
D16	Apogee kick motor	2095.	15.57	170.90	386.8
D17	Payload	2023.	47.78	39.20	185.2
D18	AI GEM noz. closure	47.	5.58	14.50	112.7
D19	GEM nosecone	230.	11.39	25.40	149.1
D20	GEM fwd. dome frags	21.	4.36	66.00	240.3
D21	GEM skirt frags	3.	0.62	66.00	240.3
D22	GEM igniter boss	15.	0.56	66.00	240.3
D23	GEM propellant frags	45.	0.56	74.10	254.7
D24	GEM nozzle assembly	564.	12.28	66.70	241.6
D25 *	Thrusting GEM	9501.	142.30	118.00	321.4
D27 *	Unignited GEM	28839.	142.30	358.00	559.8
GP1 *	GEM prop. frags	11.	0.22	113.00	314.4
GP2 *	GEM prop. frags	0.4	0.02	44.40	197.1
GP9 *	GEM non-burn prop.	205.	1.51	120.00	324.1
GC1	GEM Case frags	5.4	1.40	4.30	61.3
GC2	GEM Case frags	33.1	8.65	4.30	61.3

* Weights for these classes taken at impact following failure at 20 seconds

Table B2. Delta-GEM Splatter Parameters

Class	KE/A (ft-lb/ft^2)	Frangible factor	Mean wt. (lb)	Num. Splat. Frags		R_{max} (ft)	
				Hard	Soft	Hard	Soft
D2	10.0	0.1	0.8	0.0	0.0	1.4	0.2
D3	67.9	0.2	1.5	0.1	0.1	2.6	0.4
D4	258.3	0.2	5.1	0.3	0.3	4.0	0.8
D5	3,816.4	0.3	5.4	0.3	0.3	9.5	2.2
D6	1,524.2	0.2	0.9	0.1	0.1	7.0	1.5
D7	1,242.2	0.4	10.6	1.4	1.7	6.6	1.4
D8	5,084.7	0.4	3.4	0.5	0.5	10.4	2.5
D9	7,094.8	0.5	1.1	0.2	0.2	11.6	2.8
D10	8,241.3	0.5	8.3	1.4	1.4	12.1	3.0
D11	39,444.5	0.6	2.0	0.4	0.4	20.1	5.6
D12	10,401.7	0.4	3.7	0.8	0.8	13.1	3.3
D13	45,774.3	0.5	23.7	8.3	7.3	21.1	6.0
D14	31,184.8	0.4	4.7	1.3	1.1	18.6	5.1
D15	53,529.3	1.0	2.4	1.4	1.2	22.1	6.4
D16	313,061.8	0.5	22.9	10.6	8.0	39.1	12.9
D17	22,662.9	1.0	22.5	11.1	10.3	16.8	4.5
D18	1,678.6	0.2	3.4	0.3	0.3	7.3	1.6
D19	7,018.1	0.3	7.6	1.1	1.1	11.5	2.8
D20	4,333.9	0.2	2.3	0.6	0.7	9.9	2.3
D21	4,353.9	0.2	0.9	0.2	0.3	9.9	2.3
D22	24,101.8	0.5	1.9	0.8	0.7	17.1	4.6
D23	81,158.9	1.0	3.4	2.1	1.7	25.3	7.5
D24	41,763.6	0.3	11.9	2.5	2.2	20.4	5.8
D25 *	107,302.8	1.0	48.7	43.9	36.1	27.7	8.4
D27 *	987,302.7	1.0	84.9	113.4	78.4	56.6	20.5
GP1 *	76,955.1	1.0	1.7	1.6	0.0	24.9	0.7
GP2 *	12,119.8	1.0	0.3	0.2	0.0	13.7	0.7
GP9 *	221,877.6	1.0	7.2	5.2	1.3	35.0	7.4
GC1	233.5	0.0	1.2	0.0	0.2	3.8	3.5
GC2	231.7	0.0	2.9	0.0	4.0	3.8	11.3

* Data for these classes taken at 20 seconds

Table B3. Delta-GEM Effective Casualty Areas for Hard-Surface Impacts

Class	A_{basic} (ft^2)	A_{slide} (ft^2)	A_{bounce} (ft^2)	A_{splat} (ft^2)	A_{eff} (ft^2)	Ratio A_{eff}/A_{basic}
D2	22.67	16.52	19.34	0	42.02	1.9
D3	22.41	18.41	43.65	0	66.06	2.9
D4	55.68	31.88	92.80	1.24	148.48	2.7
D5	16.73	16.98	48.17	3.63	64.90	3.9
D6	7.31	10.68	28.69	0.34	36.00	4.9
D7	88.33	41.75	141.34	11.93	229.67	2.6
D8	12.43	0	42.13	5.70	54.56	4.4
D9	6.14	0	27.16	2.05	33.30	5.4
D10	24.87	0	64.49	21.20	89.37	3.6
D11	5.81	0	25.52	7.98	31.33	5.4
D12	12.92	0	39.34	12.97	52.26	4.0
D13	76.74	0	26.41	192.05	268.79	3.5
D14	11.85	0	17.57	27.43	39.28	3.3
D15	6.35	0	12.12	30.39	36.74	5.8
D16	33.85	0	0	408.59	442.44	13.1
D17	79.08	0	94.85	147.62	226.69	2.9
D18	19.95	0	56.36	2.46	76.31	3.8
D19	29.18	0	69.36	15.62	98.55	3.4
D20	16.15	0	14.82	6.95	30.97	1.9
D21	7.38	0	9.83	2.26	17.21	2.3
D22	7.17	0	9.68	14.21	21.38	3.0
D23	7.13	0	5.88	53.56	60.68	8.5
D24	29.54	0	19.50	64.62	94.16	3.2
D25 *	191.05	0	0	349.67	540.72	2.8
D27 *	189.63	0	0	1039.92	1229.56	6.5
GP1 *	5.58	0	0	36.47	42.05	7.5
GP2 *	4.42	0	17.93	2.27	22.35	5.1
GP9 *	9.73	0	0	179.47	189.20	19.4
GC1	12.49	13.71	36.18	0	48.67	3.9
GC2	28.20	21.86	60.77	0	88.97	3.2

* Data for these classes taken at 20 seconds

Table B4. Delta-GEM Effective Casualty Areas for Soft-Surface Impacts

Class	A_{basic} (ft^2)	A_{slide} (ft^2)	A_{bounce} (ft^2)	A_{splat} (ft^2)	A_{eff} (ft^2)	Ratio A_{eff}/A_{basic}
D2	22.67	11.80	4.84	0	34.47	1.5
D3	22.41	13.15	13.23	0	35.64	1.6
D4	55.68	22.77	36.06	0	91.74	1.6
D5	16.73	12.13	18.79	0	35.53	2.1
D6	7.31	7.63	11.62	0	18.93	2.6
D7	88.33	29.82	43.37	0	131.70	1.5
D8	12.43	0	11.19	0	23.61	1.9
D9	6.14	0	7.33	0	13.47	2.2
D10	24.87	0	14.66	0	39.54	1.6
D11	5.81	0	2.21	2.08	8.02	1.4
D12	12.92	0	1.70	3.04	15.95	1.2
D13	76.74	0	0	18.90	95.63	1.2
D14	11.85	0	0	6.70	18.55	1.6
D15	6.35	0	0	7.93	14.27	2.2
D16	33.85	0	0	87.57	121.43	3.6
D17	79.08	0	1.60	10.77	89.84	1.1
D18	19.95	0	16.68	0	36.64	1.8
D19	29.18	0	9.42	0	38.60	1.3
D20	16.15	0	0	0	16.15	1.0
D21	7.38	0	0	0	7.38	1.0
D22	7.17	0	0	3.52	10.69	1.5
D23	7.13	0	0	14.37	21.49	3.0
D24	29.54	0	0	14.04	43.58	1.5
D25 *	191.05	0	0	37.36	228.41	1.2
D27 *	189.63	0	0	213.29	402.93	2.1
GP1 *	5.58	0	0	9.96	15.54	2.8
GP2 *	4.42	0	0.01	0.57	4.99	1.1
GP9 *	9.73	0	0	49.57	59.30	6.1
GC1	12.49	9.79	15.40	0	27.88	2.2
GC2	28.20	15.62	24.56	0	52.76	1.9

* Data for these classes taken at 20 seconds

References

1. Montgomery, Robert M, and Ward, James A., "Facility Damage and Personnel Injury From Explosive Blast", April 16, 1993, RTI/5180/26-08F, Research Triangle Institute, prepared for Directorate of Safety, 45 SPW/SE, Patrick AFB, FL, and 30 SPW/SE, Vandenberg AFB, CA.

2. AF Regulation 127-100, Explosive Safety Standards, Glossary, page 142, 20 May 1983.

3. Haber, Jerold M., and Heubach, William F., "Estimation of Casualties From Impacting Debris", ACTA Inc., Technical Report No. 89-217/15-01, September 29, 1989, prepared for Department of Air Force.

4. *Handbook of Chemistry and Physics*, Chemical Rubber and Publishing Company.

5. Clements, Guy R., and Wilson, Levi T., *Analytical and Applied Mechanics*, McGraw-Hill Book Company Inc., page 237.

6. Shames, Irving H., *Engineering Mechanics: Dynamics*, Prentice-Hall Inc., 1960, page 454.

7. Document 361-83, Meteorological Group, Range Commanders Council, "Cape Canaveral Florida: Range Reference Atmosphere", February 1983, page 65.

8. Montgomery, R. M., and Ward, J. A., "Computations of Hit Probabilities From Launch-Vehicle Debris", RTI/4666/02F, September 19, 1990.

9. Ahlers, Edward B., "Fragment Hazard Study", *Minutes of Eleventh Explosive Safety Seminar, Vol. I*, Armed Services Explosive Safety Board, Washington, DC, 9-10 September 1969.

10. Kornhouser, M., *Structural Effects of Impact*, Spartan Books Inc., Baltimore, MD.

11. Henny, R. W., and Carlson, R. H., "Distribution of Natural Missiles Resulting From Cratering Explosions on Hard Rock", *Prevention and Protection Against Accidental Explosions of Munitions, Fuels and Other Hazardous Mixtures*, Annals of the NY Academy of Science, 152, Art. 1, 1968.

12. Ahlers, Edward B., "Debris Hazards, A Fundamental Study", DASA-1362, 1963.

13. Montgomery, R. M., unpublished working paper, "Casualty Expectancy", 1987.

14. Chemical Propulsion Information Agency Publication 394, Vol 1, 13 Nov 1985, Table 2-11 on page 2-21, and Figs. 2-34 and 2-35 on pages 2-80 and 2-81.

15. Baker, Wilfred E., et al., "Workbook for Predicting Pressure Wave and Fragment Effects of Exploding Propellant Tanks and Gas Storage Vessels", NASA CR-134906, September 1977.

16. Refling, O., Stern, R., Potz, C., "Review of Orbital Reentry Risk Predictions", The Aerospace Corporation, ATR-92(2835)-1, 15 July 1992.

17. Letter of transmittal from National Transportation Safety Board to RTI, January 26, 1995, by Robert Benzon, Sr. Air Safety Investigator.

18. Ward, J. A., and Montgomery, R. M., "Atlas IIAS Debris Model for HITP", RTI/5180/26-13F, September 30, 1993.

19. Ward, J. A., and Montgomery, R. M., "Delta-GEM Debris Model for HITP", RTI/5180/02F, September 30, 1992.

20. Ward, J. A., and Montgomery, R. M., "GEM Breakup Data With Case-Splitter Destruct Package", RTI/5180/26-11F, September 30, 1993.